gT(x) contribution to single spin asymmetries in SIDIS

Benić, Sanjin; Hatta, Yoshitaka; Kaushik, Abhiram; Li, Hsiang-nan

$g_T(x)$ contribution to single spin asymmetries in SIDIS

Sanjin Benić,[1] Yoshitaka Hatta,[2,3] Abhiram Kaushik,[1] and Hsiang-nan Li[4]

[1]*Department of Physics, Faculty of Science, University of Zagreb, Bijenička c. 32, 10000 Zagreb, Croatia*
[2]*Physics Department, Brookhaven National Laboratory, Upton, New York 11973, USA*
[3]*RIKEN BNL Research Center, Brookhaven National Laboratory, Upton, New York 11973, USA*
[4]*Institute of Physics, Academia Sinica, Taipei, Taiwan 11529, Republic of China*

(Received 15 September 2021; accepted 26 October 2021; published 18 November 2021)

Motivated by a novel origin of transverse single spin asymmetry (SSA) in semi-inclusive deep inelastic scattering (SIDIS) uncovered by some of us, we quantitatively investigate its impact on the theoretical understanding of the mechanism responsible for SSA. This new contribution from the quark-initiated channel first appears in two-loop perturbation theory and involves the $g_T(x)$ distribution. We point out another entirely analogous piece from the gluon-initiated channel proportional to the gluon helicity distribution $\Delta G(x)$. Both contributions are solely expressed in terms of twist-two polarized parton distribution functions and twist-two fragmentation functions in the Wandzura-Wilczek approximation, such that they can be unambiguously evaluated without introducing free parameters. We make predictions for measurements of the asymmetries A_{UT} at the future electron-ion collider (EIC), and find that A_{UT} associated with the $\sin(\phi_h - \phi_S)$, $\sin\phi_S$ and $\sin(2\phi_h - \phi_S)$ harmonics can reach up to 1–2% even at the top EIC energy.

DOI: 10.1103/PhysRevD.104.094027

I. INTRODUCTION

Recently, three of us, together with D. J. Yang, have proposed a novel mechanism for generating transverse single-spin asymmetry (SSA) in semi-inclusive deep inelastic scattering (SIDIS) $ep^\uparrow \to e'hX$ [1]. It has been demonstrated that an imaginary phase necessary for SSA can be produced purely within a parton-level cross section starting at two loops. The spin-dependent part of the cross section at high transverse momentum $P_{hT} > 1$ GeV (measured with respect to the virtual photon direction) can be schematically written as

$$\frac{d\Delta\sigma}{dP_{hT}} \sim g_T(x) \otimes H \otimes D_1(z) + \cdots, \tag{1}$$

where $g_T(x)$ is the twist-three parton distribution function (PDF) associated with a transversely polarized proton, D_1 is the unpolarized twist-two fragmentation function (FF) for the observed hadron h, and H is the hard kernel starting at $\mathcal{O}(\alpha_s^2)$ (see also an earlier related work [2]). The terms omitted in (1) are proportional to the "genuine twist-three" quark-gluon correlation functions $\sim\langle\bar\psi g F\psi\rangle$ commonly called the Efremov-Teryaev-Qiu-Sterman (ETQS) functions [3,4]. As is well known, the g_T distribution can be written as the sum of the Wandzura-Wilczek (WW) part [5] and the genuine twist-three part

$$g_T(x) = \int_x^1 \frac{dx'}{x'}\Delta q(x') + (\text{genuine twist three}), \tag{2}$$

where $\Delta q(x)$ is the twist-two polarized (helicity) quark PDF. It is a consistent truncation of the result in Ref. [1] to keep only the WW part in (2). The new source of SSA can then be entirely expressed in terms of the twist-two PDFs $\Delta q(x)$ and the twist-two FFs $D_1(z)$. This is a remarkable observation in striking contrast to the prevailing view that SSA at high-P_{hT} is explained by the ETQS functions and certain twist-three fragmentation functions (see a review [6] and references therein). Unlike these higher-twist distributions, twist-two distributions are very well constrained by global QCD analyses. Therefore, the mechanism proposed in [1] offers a unique part of SSA that can be unambiguously calculated without introducing free parameters. Moreover, in the transverse-momentum-dependent (TMD) PDF framework valid in the low-P_{hT} region ($P_{hT} \lesssim 1$ GeV), a new source of SSA proportional to the $g_{1T}(x, k_\perp)$ distribution (the TMD version of $g_T(x)$) has been identified, along with more than a dozen of new contributions involving various twist-three TMDs and FFs and hard kernels up to two loops. Again, this calls into question the prevailing view in the community

(see, e.g., [7]) that SSA at low-P_{hT} is entirely attributed to the Sivers and Collins functions.

The purpose of this paper is twofold. First, we extend the analysis of [1] to gluon-initiated channels. There exists a gluonic counterpart of $g_T(x)$, the twist-three $\mathcal{G}_{3T}(x)$ distribution [8,9] for a transversely polarized proton. Its WW part is related to the twist-two polarized gluon PDF $\Delta G(x)$. In complete analogy to (1), we find the structure

$$\frac{d\Delta\sigma}{dP_{h\perp}} \sim \mathcal{G}_{3T}(x) \otimes H_g \otimes D_1(z) \sim \Delta G(x) \otimes H_g \otimes D_1(z), \tag{3}$$

which again consists only of twist-two distributions after the WW approximation. We shall identify the two-loop diagrams that go into the hard kernel H_g and study their gauge invariance and infrared safety. Equation (3) is a novel gluon-initiated source of SSA in SIDIS to be considered jointly with the previously known mechanism which involves genuine twist-three, three-gluon correlators $\langle FgFF\rangle$ [10–12].

Second, we perform a detailed numerical analysis of SSA and make predictions for its measurements at the future Electron-Ion Collider (EIC) [13,14]. In doing so, we neglect the ETQS functions and twist-three FFs, and focus on our new contributions in order to clearly explore their importance. The results can be viewed as a baseline for future EIC measurements of SSA. Deviations from our predictions, if observed, may be attributed to genuinely twist-three effects.

This paper is organized as follows. In Sec. II, we describe the SIDIS setup and introduce kinematic variables. In Sec. III, we first review the result of [1] obtained for the quark-initiated channel, and then propose an analogous, but novel contribution to SSA in the gluon-initiated channel. In Sec. IV, we perform a detailed analysis of the two-loop diagrams and calculate the hard coefficients in all the partonic channels. In Sec. V, we implement the obtained formulas numerically and make predictions according to the kinematic coverage of the EIC. We also present results relevant to the COMPASS experiments [15]. Finally, we discuss our findings and conclude in Sec. VI. Appendices are devoted to a technical proof of the infrared finiteness of the factorization formulas at two-loop level.

II. SIDIS KINEMATICS

In this section we give a brief review of polarized SIDIS $e(l)p(P) \to e(l')h(P_h)X$ and introduce involved kinematic variables. We have in mind light hadron production specifically for $h = \pi^{\pm}$. Heavy-quark production will be studied in a separate work. The spin-dependent part of the differential cross section is given by

$$d^6\Delta\sigma = \frac{1}{2S_{ep}} \frac{d^3P_h}{(2\pi)^3 2E_h} \frac{d^3l'}{(2\pi)^3 2E_{l'}} \frac{e^4}{(Q^2)^2} L^{\mu\nu} W_{\mu\nu}, \tag{4}$$

where $S_{ep} \equiv (l+P)^2$, $Q^2 \equiv -q^2 = -(l-l')^2$, $L^{\mu\nu} = 2(l^\mu l'^\nu + l^\nu l'^\mu) - g^{\mu\nu}Q^2$ is the leptonic tensor, $W^{\mu\nu}$ is the hadronic tensor, and ν and μ are the polarization indices of the virtual photon in the amplitude and the complex-conjugate amplitude, respectively. The Bjorken variable is denoted as $x_B = Q^2/(2P\cdot q)$. We shall work in the so-called hadron frame, where the virtual photon and the proton move in the z direction with

$$q^\mu = (0,0,0,-Q), \qquad P^\mu = \left(\frac{Q}{2x_B}, 0, 0, \frac{Q}{2x_B}\right). \tag{5}$$

The incoming and outgoing leptons have the momenta

$$l^\mu = \frac{Q}{2}(\cosh\psi, \sinh\psi\cos\phi, \sinh\psi\sin\phi, -1),$$
$$l'^\mu = \frac{Q}{2}(\cosh\psi, \sinh\psi\cos\phi, \sinh\psi\sin\phi, 1), \tag{6}$$

where ϕ is the azimuthal angle relative to the z axis, and

$$\cosh\psi \equiv \frac{2x_B S_{ep}}{Q^2} - 1. \tag{7}$$

We adopt the standard variables

$$y = \frac{P\cdot q}{P\cdot l}, \qquad z_f = \frac{P\cdot P_h}{P\cdot q}, \tag{8}$$

with the relation $x_B y S_{ep} = Q^2$. Another common variable is $q_T = \sqrt{-q_t^2}$ where

$$q_t^\mu \equiv q^\mu - \frac{P_h\cdot q}{P_h\cdot P}P^\mu - \frac{P\cdot q}{P\cdot P_h}P_h^\mu. \tag{9}$$

In the present frame, the transverse part of q_t^μ reads $\vec{q}_{tT} = -\vec{P}_{hT}/z_f$. The momentum of the final state hadron can then be parametrized as

$$P_h^\mu = \frac{z_f Q}{2}\left(1 + \frac{q_T^2}{Q^2}, \frac{2q_T}{Q}\cos\chi, \frac{2q_T}{Q}\sin\chi, -1 + \frac{q_T^2}{Q^2}\right). \tag{10}$$

For the transverse spin of the incoming proton we choose

$$S_T^\mu = (0, \cos\Phi_S, \sin\Phi_S, 0). \tag{11}$$

In terms of the above variables, the differential cross section (4) takes the following Lorentz invariant form

$$\frac{d^6\Delta\sigma}{dx_B dQ^2 dz_f dq_T^2 d\phi d\chi} = \frac{\alpha_{\rm em}^2}{128\pi^4 x_B^2 S_{ep}^2 Q^2} z_f L_{\mu\nu} W^{\mu\nu}. \tag{12}$$

In practice, instead of ϕ and χ, it is more convenient to define the hadron and spin angles relative to the lepton plane,

$$\phi_h \equiv \phi - \chi, \qquad \phi_S \equiv \phi - \Phi_S, \tag{13}$$

in accordance with the Trento conventions [16]. The cross section is then a function of ϕ_h and $\Phi_S - \chi = \phi_h - \phi_S$. The dependence on ϕ_h can be factored out by decomposing the hadron tensor $W^{\mu\nu}$ using the following set of vectors [17],

$$\begin{aligned} T^\mu &= \frac{1}{Q}(q^\mu + 2x_B P^\mu), \\ X^\mu &= \frac{1}{q_T}\left[\frac{P_h^\mu}{z_f} - q^\mu - \left(1 + \frac{q_T^2}{Q^2}\right)x_B P^\mu\right], \\ Y^\mu &= \epsilon^{\mu\nu\rho\sigma} Z_\nu X_\rho T_\sigma, \\ Z^\mu &= -\frac{q^\mu}{Q}, \end{aligned} \tag{14}$$

which form nine independent tensors, $\mathcal{V}_k^{\mu\nu}$ (see [17] for explicit expressions), and their inverses, $\tilde{\mathcal{V}}_k^{\mu\nu}$. Among them, the following six symmetric tensors [17] contribute to the decomposition of $W^{\mu\nu}$,

$$\begin{aligned} \tilde{\mathcal{V}}_1^{\mu\nu} &= \frac{1}{2}(2T^\mu T^\nu + X^\mu X^\nu + Y^\mu Y^\nu), \\ \tilde{\mathcal{V}}_2^{\mu\nu} &= T^\mu T^\nu, \\ \tilde{\mathcal{V}}_3^{\mu\nu} &= -\frac{1}{2}(T^\mu X^\nu + X^\mu T^\nu), \\ \tilde{\mathcal{V}}_4^{\mu\nu} &= \frac{1}{2}(X^\mu X^\nu - Y^\mu Y^\nu), \\ \tilde{\mathcal{V}}_8^{\mu\nu} &= -\frac{1}{2}(T^\mu Y^\nu + Y^\mu T^\nu), \\ \tilde{\mathcal{V}}_9^{\mu\nu} &= \frac{1}{2}(X^\mu Y^\nu + Y^\mu X^\nu). \end{aligned} \tag{15}$$

With these tensors we can write

$$L_{\mu\nu} W^{\mu\nu} = Q^2 \sum_{k=1,\ldots,4,8,9} \mathcal{A}_k(\phi_h)[W_{\rho\sigma}\tilde{\mathcal{V}}_k^{\rho\sigma}], \tag{16}$$

where

$$\mathcal{A}_k(\phi_h) = L_{\mu\nu}\mathcal{V}_k^{\mu\nu}/Q^2, \tag{17}$$

have the explicit expressions

$$\begin{aligned} \mathcal{A}_1(\phi_h) &= 1 + \cosh^2\psi, \\ \mathcal{A}_2(\phi_h) &= -2, \\ \mathcal{A}_3(\phi_h) &= -\cos\phi_h \sinh 2\psi, \\ \mathcal{A}_4(\phi_h) &= \cos 2\phi_h \sinh^2\psi, \\ \mathcal{A}_8(\phi_h) &= -\sin\phi_h \sinh 2\psi, \\ \mathcal{A}_9(\phi_h) &= \sin 2\phi_h \sinh^2\psi. \end{aligned} \tag{18}$$

We are thus led to the representation (see for example [18])

$$\begin{aligned} \frac{d^6\Delta\sigma}{dx_B dQ^2 dz_f dq_T^2 d\phi d\chi} &= \sin(\phi_h - \phi_S)(\mathcal{F}_1 + \mathcal{F}_2\cos\phi_h + \mathcal{F}_3\cos 2\phi_h) + \cos(\phi_h - \phi_S)(\mathcal{F}_4\sin\phi_h + \mathcal{F}_5\sin 2\phi_h) \\ &= [F^{\sin(\phi_h-\phi_S)}\sin(\phi_h - \phi_S) + F^{\sin(2\phi_h-\phi_S)}\sin(2\phi_h - \phi_S) + F^{\sin\phi_S}\sin\phi_S \\ &\quad + F^{\sin(3\phi_h-\phi_S)}\sin(3\phi_h - \phi_S) + F^{\sin(\phi_h+\phi_S)}\sin(\phi_h + \phi_S)], \end{aligned} \tag{19}$$

with

$$\begin{aligned} F^{\sin(\phi_h-\phi_S)} &= \mathcal{F}_1, \\ F^{\sin(2\phi_h-\phi_S)} &= \frac{\mathcal{F}_2 + \mathcal{F}_4}{2}, \\ F^{\sin\phi_S} &= \frac{-\mathcal{F}_2 + \mathcal{F}_4}{2}, \\ F^{\sin(3\phi_h-\phi_S)} &= \frac{\mathcal{F}_3 + \mathcal{F}_5}{2}, \\ F^{\sin(\phi_h+\phi_S)} &= \frac{-\mathcal{F}_3 + \mathcal{F}_5}{2}. \end{aligned} \tag{20}$$

The Fourier components $\sin(\phi_h - \phi_S)$ and $\sin(\phi_h + \phi_S)$ are referred to as the Sivers and Collins asymmetries, respectively. While we continue to use this nomenclatures, we emphasize that the new mechanism, which contributes to these asymmetries and will be studied in detail below, has nothing to do with the Sivers and Collins functions, or their collinear twist-three counterparts.

III. NEW CONTRIBUTIONS TO SSA

In this section we first recapitulate the $g_T(x)$ contribution to SSA discussed in [1], and apply the so-called Wandzura-Wilczek (WW) approximation to simplify the result. We then derive another new contribution to SSA due to the gluonic counterpart of g_T.

A. Quark-initiated channel

In [1], it has been shown that the imaginary phase necessary for SSA in SIDIS can come from the hard kernel in perturbation theory starting at two loops, and all the relevant two-loop diagrams have been identified. However, only the quark (and antiquark) initiated channel was considered there. In this channel, motivated by the structure (1), we factorize the fragmentation function out of the hadronic tensor $W_{\mu\nu}$ as

$$W_{\mu\nu} = \sum_{a=q,\bar{q},g} \int \frac{dz}{z^2} D_1^a(z) w_{\mu\nu}^a, \tag{21}$$

where we have taken into account the fact that the observed hadron can also come from the fragmentation of a radiated gluon in the final state. The result of [1] reads (suppressing the label a for simplicity)

$$\begin{aligned} w_{\mu\nu} = {} & \frac{M_N}{2} \int dx g_T(x) \mathrm{Tr}[\gamma_5 \not{S}_T S_{\mu\nu}^{(0)}(xP)] - \frac{M_N}{4} \int dx \tilde{g}(x) \mathrm{Tr}\left[\gamma_5 \not{P} S_T^\alpha \frac{\partial S_{\mu\nu}^{(0)}(k)}{\partial k_T^\alpha}\bigg|_{k=xP}\right] \\ & + \frac{iM_N}{4} \int dx_1 dx_2 \mathrm{Tr}\left[\left(\not{P} \epsilon^{\alpha PnS_T} \frac{G_F(x_1,x_2)}{x_1 - x_2} + i\gamma_5 \not{P} S_T^\alpha \frac{\tilde{G}_F(x_1,x_2)}{x_1 - x_2}\right) S_{\mu\nu\alpha}^{(1)}(x_1 P, x_2 P)\right], \end{aligned} \tag{22}$$

in which M_N is the proton mass, and Tr denotes trace over colors and Dirac indices. Our conventions are $\epsilon_{0123} = +1$, $\gamma_5 = i\gamma^0\gamma^1\gamma^2\gamma^3$ and $\epsilon^{\alpha PnS} = \epsilon^{\alpha\beta\rho\lambda} P_\beta n_\rho S_{T\lambda}$ with the lightlike vector n^μ satisfying $n^2 = 1$ and $n \cdot P = 1$. The $g_T(x)$ distribution function is defined as

$$\begin{aligned} & \int \frac{d\lambda}{2\pi} e^{i\lambda x} \langle P S_T | \bar{\psi}_j(0) [0, \lambda n] \psi_i(\lambda n) | P S_T \rangle \\ & \quad = \frac{M_N}{2} (\gamma_5 \not{S}_T)_{ij} g_T(x) + \ldots. \end{aligned} \tag{23}$$

while $G_F(x_1, x_2)$ and $\tilde{G}_F(x_1, x_2)$ are the ETQS functions (We follow the notation of Ref. [19] where explicit definitions can be found). The "kinematical" distributions $\tilde{g}(x)$ and $g_T(x)$ are related through the QCD equation of motion

$$g_T(x) + \frac{\tilde{g}(x)}{2x} = \int dx' \frac{G_F(x,x') + \tilde{G}_F(x,x')}{x - x'}. \tag{24}$$

The hard matrix elements $S_{\mu\nu}^{(0)}(xP)$ and $S_{\mu\nu\alpha}^{(1)}(x_1 P, x_2 P)$ are computable in perturbation theory. As observed in [1], the first nonzero contribution to $S^{(0)}$ appears at two loops, $S^{(0)} \propto \alpha_s^2$, and $S^{(1)}$ is obtained from $S^{(0)}$ by attaching an extra gluon in all possible ways. Two representative diagrams contributing to $S^{(0)}$ are shown in Fig. 1. The crosses denote on-shell lines that lead to an imaginary phase via the Cutkosky rules. We note that Ref. [2] arrived at essentially the same structure as (22), but did not specify the hard kernels $S^{(0,1)}$.

We shall compute $w_{\mu\nu}$ in the WW approximation, namely, by systematically neglecting genuine twist-three distributions everywhere. This is a consistent approximation in the sense that it preserves both QED and QCD gauge invariance. In this approximation, we may write[1]

$$\begin{aligned} & g_T(x) \to \int_x^1 \frac{dx'}{x'} (\Delta q(x') + \Delta\bar{q}(x)), \\ & \tilde{g}(x) \approx -2x g_T(x), \end{aligned} \tag{25}$$

where $\Delta q(x)$ and $\Delta\bar{q}(x)$ are the standard twist-two polarized quark and antiquark distributions. Moreover, the first two lines in (22) can be combined into

$$w_{\mu\nu} \approx \frac{M_N}{2} \int dx g_T(x) S_T^\alpha \left(\frac{\partial}{\partial k_T^\alpha} \mathrm{Tr}[\gamma_5 \not{k} S_{\mu\nu}^{(0)}(k)]\right)_{k=xP}. \tag{26}$$

We thus arrive at the structure mentioned in the Introduction,

$$d\Delta\sigma \sim (\Delta q(x) + \Delta\bar{q}(x)) \otimes H \otimes D_1(z). \tag{27}$$

The above formulas hold for each quark flavor. In practice, we must sum over flavors weighted by the quark electromagnetic charge. In physical cross sections, we thus apply $g_T(x) \to \sum_f e_f^2 g_{Tf}(x)$ where g_{Tf} is given by (25) for each quark flavor f.

Let us compare (27) with the conventional contribution from the ETQS function [19–21] which schematically reads[2]

[1] $\Delta\bar{q}(x)$ is formally related to the operator definition of $g_T(x)$ in the negative support region $0 > x > -1$. We have checked that the antiquark contribution can be effectively included via the replacement (25) in the physical region $1 > x > 0$ using the same hard kernel.

[2] To avoid confusion, we note that the G_F and $\tilde{G}_F$ pieces in (22) are not the conventional ETQS contribution quoted here, but rather its $\mathcal{O}(\alpha_s)$ corrections.

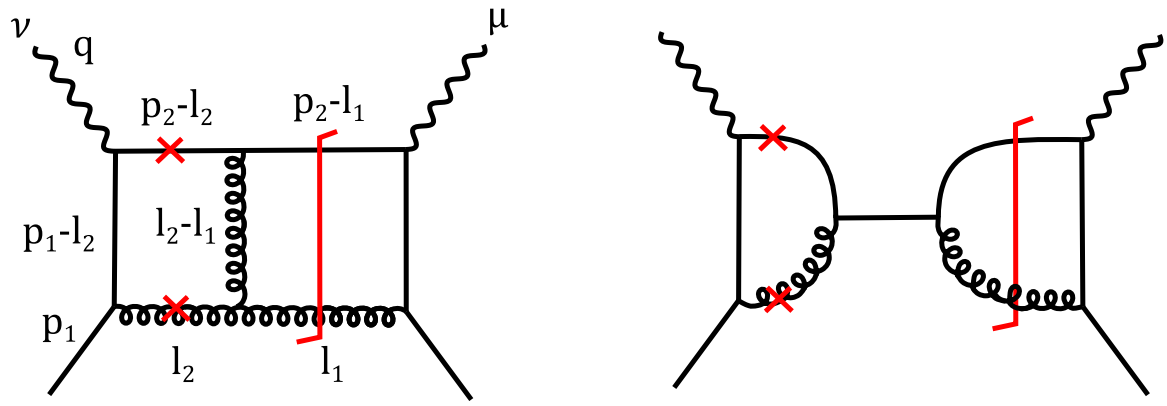

FIG. 1. Prototype two-loop diagrams contributing to SSA in the quark initiated channel, where the crosses denote the cuts needed to generate an imaginary phase, the vertical line is the final state cut, and $p_1 = xP$ is the incoming quark momentum.

$$d\Delta\sigma_{\mathrm{ETQS}} \sim G_F(x,x') \otimes H' \otimes D_1(z). \tag{28}$$

Since $H \sim \mathcal{O}(\alpha_s^2)$ and $H' \sim \mathcal{O}(\alpha_s)$, naively the former is parametrically suppressed by a factor of α_s. However, the definition $G_F \sim \langle \bar{\psi} g F \psi \rangle$ explicitly contains the coupling g which actually comes from perturbative diagrams. That is, some suppression associated with the coupling g goes into G_F in the convention (28). As for the soft part, both conceptually and practically, we have a far better grasp of twist-two distributions than twist-three distributions: Δq and D_1 have been well constrained thanks to a wealth of experimental data and global QCD analyses, whereas the ETQS functions are still poorly constrained. These considerations make (27) a new and attractive source of SSA that can be unambiguously calculated without introducing any free parameters. The main goal of this paper is to carry out such a calculation, both analytically and numerically. But before doing so, let us point out that an entirely analogous contribution exists in the gluon-initiated channel.

B. Gluon-initiated channel

The gluonic counterpart of $g_T(x)$ for a transversely polarized proton is defined as [8,9,22]

$$\int \frac{d\lambda}{2\pi} e^{ix\lambda} \langle PS_T | F^{n\alpha}(0)[0,\lambda n] F^{n\beta}(\lambda n) | PS_T \rangle = iM_N x \mathcal{G}_{3T}(x) \epsilon^{n\alpha\beta S_T} + \ldots. \tag{29}$$

Similar to $g_T(x)$, it can be written as the sum of the WW part and the genuine twist-three part,

$$\mathcal{G}_{3T}(x) = \frac{1}{2}\int_x^1 \frac{dx'}{x'} \Delta G(x') + (\text{genuine twist three}), \tag{30}$$

where the WW part is related to the polarized (helicity) gluon PDF $\Delta G(x)$, and the genuine twist-three part consists of three-gluon correlators $\sim\langle FFF\rangle$. Their full expressions can be found in [9].

The $\mathcal{G}_{3T}$ distribution appeared in the previous calculation of the double spin asymmetry A_{LT} in proton-proton collisions $p^{\rightarrow} p^{\uparrow} \to hX$ [23]. The cross section formula derived in [23] can be straightforwardly adapted to the case of single spin asymmetry in SIDIS $ep^{\uparrow} \to hX$. Writing the hadronic tensor as

$$W^g_{\mu\nu} = \sum_{a=q,\bar{q}} \int \frac{dz}{z^2} D_1^a(z) w^{g,a}_{\mu\nu}, \tag{31}$$

we find (see (17) and (25) of [23])

$$w^g_{\mu\nu} = iM_N \int \frac{dx}{x} \mathcal{G}_{3T}(x) \epsilon^{n\alpha\beta S_T} S^{(0)\alpha'\beta'}_{\mu\nu}(xP) \omega_{\alpha'\alpha}\omega_{\beta'\beta} - iM_N \int \frac{dx}{x^2} \tilde{g}(x) (g_T^{\beta\lambda} \epsilon^{\alpha PnS_T} - g_T^{\alpha\lambda} \epsilon^{\beta PnS_T}) \left(\frac{\partial S^{(0)}_{\mu\nu\alpha\beta}(k)}{\partial k^\lambda}\right)_{k=xP} - \frac{1}{2}\int \frac{dx_1 dx_2}{x_1 x_2} M_F^{\alpha\beta\gamma}(x_1,x_2) \frac{S^{(1)\alpha'\beta'\gamma'}(x_1,x_2)}{x_2 - x_1} \omega_{\alpha'\alpha}\omega_{\beta'\beta}\omega_{\gamma'\gamma}, \tag{32}$$

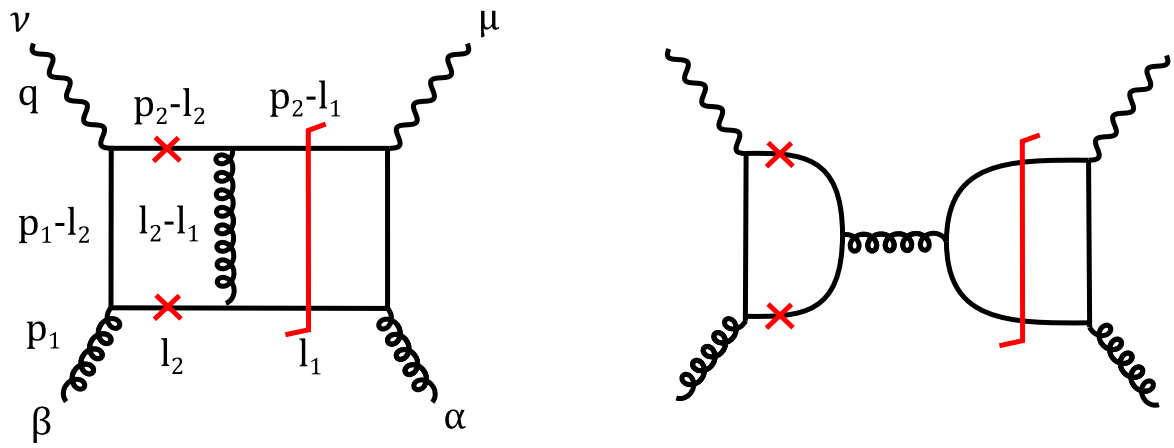

FIG. 2. Prototype two-loop diagrams contributing to SSA in the gluon initiated channel, where the crosses denote the cuts needed for SSA and the vertical line is the final state cut. The right diagram with a s-channel gluon does not contribute due to Furry's theorem.

where $g_T^{\mu\nu} = g^{\mu\nu} - P^\mu n^\nu - n^\mu P^\nu$ and $\omega^{\mu\nu} = g^{\mu\nu} - P^\mu n^\nu$ are the projectors to the transverse space. $\tilde{g}(x)$ is again a kinematical function with its precise definition given in [9] (see also [22] where it is called $\Delta G_T^{(1)}(x)$). M_F denotes the three-gluon correlators $\langle FFF\rangle$ (see (19) of [23]). The hard part also starts at two loops, $S^{(0)} \sim \alpha_s^2$, whose diagrams have the same topology as in the quark-initiated channel. A representative diagram is displayed on the left hand side of Fig. 2, and $S^{(1)}$ is obtained by attaching a gluon to this diagram in all possible ways. The diagram on the right, which is an analog of the right diagram in Fig. 1, does not contribute due to Furry's theorem. Note that in the computation of A_{LT} in Ref. [23], the imaginary phase comes from the definition of $\Delta G(x)$ for the longitudinally polarized proton. That is, the nonpole part of the hard kernel was calculated. In the present case, the imaginary phase comes from propagator poles in the hard kernel $S_{\alpha\beta}^{\mu\nu}$, and this is why two-loop diagrams are needed.

In the WW approximation, we may write

$$\mathcal{G}_{3T}(x) \approx \frac{1}{2}\int_x^1 \frac{dx'}{x'}\Delta G(x'), \qquad \tilde{g}(x) \approx x^2 \mathcal{G}_{3T}(x), \tag{33}$$

and neglect the third line of (32). We thus arrive at a new contribution to SSA of the form (3) which consists only of twist-two distributions. For light-hadron production, this contribution is suppressed compared to the quark one discussed earlier. However, for SSA in productions of heavy systems such as open charm and J/ψ, it is expected to play a more important role.

IV. COMPUTATION OF THE HARD PART: QUARK-INITIATED CHANNEL

In this and the next sections, we embark on an analysis of the two-loop diagrams for the quark and gluon initiated channels, respectively. The calculation is rather involved, especially because nontrivial cancellations of infrared divergences are in demand. In the end, we shall have infrared safe formulas that can be straightforwardly evaluated numerically.

A. Quark-fragmenting channel

In Fig. 1, either a quark or a gluon in the final state fragments into the observed hadron. For definiteness, we focus on the former process below. The treatment of the latter is basically analogous, and will be included only in the final formulas. The hard factor $S_{\mu\nu}^{(0)}$ for the quark-initiated and quark-fragmenting channel explicitly reads [1]

$$S^{(0)\mu\nu}(k) = -\frac{g^4}{2N_c}(2\pi)\delta((k+q-p_q)^2)\int\frac{d^4l_2}{(2\pi)^4}(2\pi)\delta(l_2^2)(2\pi)\delta((k+q-l_2)^2)$$
$$\times\{iA^{\alpha\mu}(k+q-p_q)\bar{M}_{\alpha\beta}(k+q-p_q,l_2)A^{\nu\beta}(l_2) - iA^{\alpha\mu}(l_2)\bar{M}_{\alpha\beta}(l_2,k+q-p_q)A^{\nu\beta}(k+q-p_q)\}, \tag{34}$$

where k and p_q are the momenta of incoming and outgoing quarks, respectively, and

$$\bar{M}_{\alpha\beta}(k+q-p_q,l_2) = \frac{N_c(N_c^2-1)}{4}\not{p}_q\left[-\frac{V_{\alpha\beta\rho}(k+q-p_q,l_2)\gamma^\rho}{(k+q-p_q-l_2)^2}+\frac{N_c^2-1}{N_c^2}\gamma_\alpha\frac{\not{k}+\not{q}}{(k+q)^2}\gamma_\beta-\frac{1}{N_c^2}\gamma_\beta\frac{\not{p}_q-\not{l}_2}{(p_q-l_2)^2}\gamma_\alpha\right](\not{k}+\not{q}-\not{l}_2), \tag{35}$$

$$V_{\alpha\beta\rho}(k+q-p_q,l_2) = g_{\alpha\beta}(l_2+k+q-p_q)_\rho + g_{\alpha\rho}(l_2-2(k+q-p_q))_\beta + g_{\rho\beta}(k+q-p_q-2l_2)_\alpha, \tag{36}$$

$$A^{\alpha\mu}(k+q-p_q) = \gamma^\alpha\frac{\not{p}_q-\not{q}}{(p_q-q)^2}\gamma^\mu+\gamma^\mu\frac{\not{k}+\not{q}}{(k+q)^2}\gamma^\alpha, \tag{37}$$

$$A^{\nu\beta}(l_2) = \gamma^\nu\frac{\not{k}-\not{l}_2}{(k-l_2)^2}\gamma^\beta+\gamma^\beta\frac{\not{k}+\not{q}}{(k+q)^2}\gamma^\nu. \tag{38}$$

Equation (34) represents the sum of $12 = 2\times3\times2$ diagrams, two of which are shown in Fig. 1. One can easily recognize the part of diagrams each piece of Feynman rules corresponds to. In (35) we have performed a color trace, while the Dirac trace is yet to be done. There are three δ-functions, one for the unobserved gluon in the final state $\delta((k+q-p_q)^2)$, and the other two come from the poles of internal propagators (denoted by the crosses in Fig. 1).

Eventually we shall take the collinear limit $k\to p_1\equiv xP$ in these expressions and introduce shorthand notations $p_2\equiv p_1+q$ and $l_1\equiv p_2-p_q$, the latter being the momentum of the unobserved gluon in Fig. 1. However, this has to be done with some care because the limit does not commute with the k_T-derivative acting on the hard kernel in (26). Let us define

$$S^{(0)}_{\mu\nu}(k) = g^4(2\pi)\delta((k+q-p_q)^2)\int\frac{d^2\vec{l}_{2T}dl_2^+}{(2\pi)^3 2l_2^+}(2\pi)\delta((k+q-l_2)^2)\hat{S}^{(0)}_{\mu\nu}(k), \tag{39}$$

where $\hat{S}^{(0)}_{\mu\nu}(k)$ can be read off from (34). We first convert the k_T-derivatives of the δ-functions to the x-derivatives as [24]

$$S_T^\alpha\left(\frac{\partial}{\partial k_T^\alpha}\delta((k+q-p_q)^2)\right)_{k=p_1} = -\frac{p_q\cdot S_T}{p_1\cdot(p_2-p_q)}x\frac{\partial}{\partial x}\delta((p_2-p_q)^2) = \frac{l_1\cdot S_T}{p_1\cdot l_1}x\frac{\partial}{\partial x}\delta(l_1^2), \tag{40}$$

$$S_T^\alpha\left(\frac{\partial}{\partial k_T^\alpha}\delta((k+q-l_2)^2)\right)_{k=p_1} = -\frac{l_2\cdot S_T}{p_1\cdot(p_2-l_2)}x\frac{\partial}{\partial x}\delta((p_2-l_2)^2), \tag{41}$$

and then use integration by parts to shuffle the x-derivatives from the δ-functions to the hard factor $\hat{S}^{(0)}_{\mu\nu}$. From the term $\partial\delta(l_1^2)/\partial x$ in (40), we get a term with $\partial g_T/\partial x$ and a term with

$$\frac{\partial}{\partial x}\left[x\int\frac{d^2\vec{l}_{2T}dl_2^+}{(2\pi)^3 2l_2^+}\ldots\right]. \tag{42}$$

From the term $\partial\delta((p_2-l_2)^2)/\partial x$ in (41), we get a term with $\partial\delta(l_1^2)/\partial x$, a term with $\partial g_T/\partial x$ and a term with

$$\frac{\partial}{\partial x}\{\mathrm{Tr}[\gamma_5\not{p}_1\hat{S}^{(0)}_{\mu\nu}(p_1)]\}. \tag{43}$$

We further convert $\partial\delta(l_1^2)/\partial x$ to a term with $\partial g_T/\partial x$ and a term like (42). The two resulting terms with $\partial g_T/\partial x$ cancel. In total, we are led to

$$
\begin{aligned}
w_{\mu\nu} &= \frac{M_N}{2}\int dx g_T(x) S_T^\alpha \left(\frac{\partial}{\partial k_T^\alpha}\mathrm{Tr}[\gamma_5 \not{k} S^{(0)}_{\mu\nu}(k)]\right)_{k=p_1} \\
&= \frac{M_N}{2}\int dx (2\pi)\delta(l_1^2)\left[-x\frac{\partial g_T(x)}{\partial x}\int \frac{d^2\vec{l}_{2T}dl_2^+}{(2\pi)^3 2l_2^+}\frac{l_1\cdot S_T}{p_1\cdot l_1}(2\pi)\delta((p_2-l_2)^2)g^4\mathrm{Tr}[\gamma_5 \not{p}_1 \hat{S}^{(0)}_{\mu\nu}(p_1)]\right. \\
&\quad - g_T(x)\frac{\partial}{\partial x}\left\{x\int \frac{d^2\vec{l}_{2T}dl_2^+}{(2\pi)^3 2l_2^+}\left[\frac{l_1\cdot S_T}{p_1\cdot l_1}+\frac{l_2\cdot S_T}{p_1\cdot(p_2-l_2)}\right](2\pi)\delta((p_2-l_2)^2)g^4\mathrm{Tr}[\gamma_5 \not{p}_1 \hat{S}^{(0)}_{\mu\nu}(p_1)]\right\} \\
&\quad + x g_T(x)\int \frac{d^2\vec{l}_{2T}dl_2^+}{(2\pi)^3 2l_2^+}\frac{l_2\cdot S_T}{p_1\cdot(p_2-l_2)}(2\pi)\delta((p_2-l_2)^2)g^4\frac{\partial}{\partial x}\{\mathrm{Tr}[\gamma_5 \not{p}_1 \hat{S}^{(0)}_{\mu\nu}(p_1)]\} \\
&\quad \left. + g_T(x)\int \frac{d^2\vec{l}_{2T}dl_2^+}{(2\pi)^3 2l_2^+}(2\pi)\delta((p_2-l_2)^2)g^4 S_T^\alpha\left(\frac{\partial}{\partial k_T^\alpha}\mathrm{Tr}[\gamma_5 \not{k}\hat{S}^{(0)}_{\mu\nu}(k)]\right)_{k=p_1}\right],
\end{aligned}
\tag{44}
$$

for which l_1 is fixed through momentum conservation as $l_1 = p_2 - p_q$.

A general proof on both QED and QCD gauge invariance of the hadronic tensor (22) was given in [1]. It was also realized that the first two terms in (22) contain infrared divergence separately when the momentum l_2 becomes collinear to the incoming quark line (see Fig. 1), but the divergences cancel exactly. Now that we have written the original formula in a significantly different form (44), it is a nontrivial task to check that (44) is gauge invariant and divergence free. In Appendix A, we show that this is indeed the case, but only after summing all the lines of (44). Knowing where divergences are hidden in intermediate expressions greatly helps a numerical analysis.

B. Calculation of the hard coefficients

With (16), (21) and (44), the polarized cross section (12) takes the following form

$$
\begin{aligned}
\frac{d^6\Delta\sigma}{dx_B dQ^2 dz_f dq_T^2 d\phi d\chi} &= \frac{\alpha_{\mathrm{em}}^2\alpha_S^2 M_N}{16\pi^2 x_B^2 S_{ep}^2 Q^2}\sum_k \mathcal{A}_k \int\frac{dx}{x}\int\frac{dz}{z}(2\pi)\delta\left(\frac{q_T^2}{Q^2}-\left(1-\frac{1}{\hat{x}}\right)\left(1-\frac{1}{\hat{z}}\right)\right)\sum_f e_f^2 D_f(z) \\
&\quad\times\left\{-x^2\frac{\partial g_{Tf}(x)}{\partial x}\frac{l_1\cdot S_T}{p_1\cdot l_1}\int\frac{d^2\vec{l}_{2T}dl_2^+}{(2\pi)^3 2l_2^+}(2\pi)\delta((p_2-l_2)^2)\mathrm{Tr}[\gamma_5 \not{p}_1 \hat{S}^{(0)}_{\mu\nu}(p_1)\tilde{\mathcal{V}}_k^{\mu\nu}]\right. \\
&\quad - x g_{Tf}(x)\frac{\partial}{\partial x}\left\{x\int\frac{d^2\vec{l}_{2T}dl_2^+}{(2\pi)^3 2l_2^+}(2\pi)\delta((p_2-l_2)^2)\left[\frac{l_1\cdot S_T}{p_1\cdot l_1}+\frac{l_2\cdot S_T}{p_1\cdot(p_2-l_2)}\right]\mathrm{Tr}[\gamma_5 \not{p}_1 \hat{S}^{(0)}_{\mu\nu}(p_1)\tilde{\mathcal{V}}_k^{\mu\nu}]\right\} \\
&\quad + x g_{Tf}(x)\int\frac{d^2\vec{l}_{2T}dl_2^+}{(2\pi)^3 2l_2^+}(2\pi)\delta((p_2-l_2)^2)\frac{l_2\cdot S_T}{p_1\cdot(p_2-l_2)}x\frac{\partial}{\partial x}\{\mathrm{Tr}[\gamma_5 \not{p}_1 \hat{S}^{(0)}_{\mu\nu}(p_1)\tilde{\mathcal{V}}_k^{\mu\nu}]\} \\
&\quad \left. + x g_{Tf}(x)\int\frac{d^2\vec{l}_{2T}dl_2^+}{(2\pi)^3 2l_2^+}(2\pi)\delta((p_2-l_2)^2)\left(\frac{\partial}{\partial k_T^\alpha}\mathrm{Tr}[\gamma_5 \not{k} S_T^\alpha \hat{S}^{(0)}_{\mu\nu}(k)\tilde{\mathcal{V}}_k^{\mu\nu}]\right)_{k=p_1}\right\},
\end{aligned}
\tag{45}
$$

where the common notations $\hat{x}\equiv x_B/x$ and $\hat{z}\equiv z_f/z$ have been introduced. We have included a flavor summation with explicit charges e_f^2, as commented after (27). Equation (45) contains two δ-function constraints with the first one $\delta(\frac{q_T^2}{Q^2}-\cdots)$ originating from $\delta(l_1^2)$. Solving the conditions $l_1^2=(p_2-p_q)^2=0$ and $p_q^2=(p_2-l_1)^2=0$, we find two roots

$$
l^+_{1(a_1)} = \frac{p_2^+}{2}(1+a_1\Delta_1), \qquad l^-_{1(a_1)} = \frac{p_2^-}{2}(1-a_1\Delta_1), \qquad \Delta_1 = \sqrt{1-\frac{4l_{1T}^2}{p_2^2}}, \qquad a_1=\pm 1. \tag{46}
$$

Recalling the definition $z_f = P\cdot P_h/P\cdot q$, we have $p_q^- = p_2^- - l_1^- = \hat{z}q^-$, whose matching onto (46) leads to $\Delta_1 = a_1(2\hat{z}-1)$. Since $\Delta_1>0$, the two roots $l^+_{1(a_1)}$ effectively split the z integration according to the constraint $a_1(2\hat{z}-1)>0$:

$$\int dz = \sum_{a_1=\pm} \int dz \theta(a_1(2\hat{z}-1)). \tag{47}$$

The second δ-function sets $(p_2 - l_2)^2 = 0$, which, together with the condition $l_2^2 = 0$, give two roots

$$l^+_{2(a_2)} = \frac{p_2^+}{2}(1 + a_2\Delta_2), \qquad l^-_{2(a_2)} = \frac{p_2^-}{2}(1 - a_2\Delta_2),$$
$$\Delta_2 = \sqrt{1 - \frac{4l_{2T}^2}{p_2^2}}, \qquad a_2 = \pm 1. \tag{48}$$

We are allowed to perform the l_2 integrals as

$$\int \frac{d^2\vec{l}_{2T} dl_2^+}{(2\pi)^3 2l_2^+}(2\pi)\delta((p_2 - l_2)^2)$$
$$= \sum_{a_2=\pm} \int \frac{d^2\vec{l}_{2T}}{(2\pi)^2} \frac{1}{2p_2^2\Delta_2} \int_{-\infty}^{\infty} dl_2^+ \delta(l_2^+ - l^+_{2(a_2)})$$
$$= \frac{1}{32\pi^2} \sum_{a_2=\pm} \int_0^1 d\Delta_2 \int_0^{2\pi} d\phi_2. \tag{49}$$

In the last equality, we have switched to the polar coordinate and changed the integration variable from l_{2T} to Δ_2. This facilitates the computation significantly because we do not have to integrate over rational functions involving square roots.

Next, we compute the Dirac traces using FEYNCALC [25] and apply the x- and k_T-derivatives to the 3rd, 4th, and 5th lines of (45), which have to be done carefully. Note that the x-derivative acts outside the l_2 integral in the 3rd line. We can only evaluate $\delta((p_2 - l_2)^2)$ and the evaluation of $\delta(l_1^2)$ cannot be performed before taking the x-derivative. In the 4th (5th) line the x (k_T^α)-derivative is within the l_2 integral and so both $p_2 - l_2$ and l_1 are put on-shell after the derivatives are taken.

The subsequent integrals over ϕ_2 and Δ_2 are the most cumbersome part of the entire calculation. The nontrivial angular dependence comes from the propagator denominators

$$(l_1 - l_2)^2 = -\left[\frac{p_2^2}{4}(a_1\Delta_1 - a_2\Delta_2)^2 + (\vec{l}_{1T} - \vec{l}_{2T})^2\right],$$
$$(p_2 - l_1 - l_2)^2 = -\left[\frac{p_2^2}{4}(a_1\Delta_1 + a_2\Delta_2)^2 + (\vec{l}_{1T} + \vec{l}_{2T})^2\right], \tag{50}$$

leading to a $\cos(\phi_1 - \phi_2)$ term, while in the numerator, after taking Dirac traces, we are left with powers of $\cos(\phi_1 - \phi_2)$ as well as linear terms of the forms $\sin(\phi_2 - \Phi_S)$ and $\cos(\phi_2 - \Phi_S)$ arising from $\epsilon^{Pnl_2S_T}$ and $l_2 \cdot S_T$, respectively. We list the formulas used to carry out such integrals in Appendix C. After the ϕ_2 integration, the $k = 1, 2, 3, 4$ terms are proportional to

$$\epsilon^{l_{1T}S_T} = -\frac{1}{z}\epsilon^{P_{hT}S_T} = -q_T\hat{z}\sin(\Phi_S - \chi), \tag{51}$$

where $\epsilon^{12} = -\epsilon^{21} = 1$, and the $k = 8, 9$ terms are proportional to

$$l_1 \cdot S_T = -\vec{l}_{1T} \cdot \vec{S}_T = \frac{1}{z}\vec{P}_{hT} \cdot \vec{S}_T = q_T\hat{z}\cos(\Phi_S - \chi). \tag{52}$$

In the individual lines of (45), the integral over the modulus l_{2T} has a singularity when $l_{2T} \to 0$ (or when $\Delta_2 \to 1$), and when $a_2 = -1$. However, as we will demonstrate in Appendix A, the total expression is finite because of the QCD Ward identity. Therefore, we first compute the ϕ_2 integrals for each line separately, sum up the results from all the lines and perform the l_{2T} (Δ_2) integration afterwards. One notable feature is that the loop integration yields in principle a different expression for each of the four combinations of the roots (a_1, a_2). However, we have found that after the summation over a_2 the results are independent of a_1. This is an important consistency check as it effectively ensures that, after all, the split (47) is not necessary and we are back to the ordinary z integral over a complete domain allowed by kinematics.

The above discussion is for the quark-initiated and quark-fragmenting channel. We have repeated the whole procedure for the quark-initiated and gluon-fragmenting channel. Adding the two pieces, we finally arrive at the total result

$$\frac{d^6\Delta\sigma}{dx_B dQ^2 dz_f dq_T^2 d\phi d\chi}$$
$$= \frac{\alpha_{\rm em}^2\alpha_S^2 M_N}{16\pi^2 x_B^2 S_{ep}^2 Q^2} \sum_k \mathcal{A}_k \mathcal{S}_k \int_{x_{\min}}^1 \frac{dx}{x} \int_{z_{\min}}^1 \frac{dz}{z} \delta\left(\frac{q_T^2}{Q^2} - \left(1 - \frac{1}{\hat{x}}\right)\left(1 - \frac{1}{\hat{z}}\right)\right)$$
$$\times \sum_f e_f^2 \left[D_f(z)x^2 \frac{\partial g_{Tf}(x)}{\partial x}\Delta\hat{\sigma}_{Dk}^{qq} + D_f(z)x g_{Tf}(x)\Delta\hat{\sigma}_k^{qq} + D_g(z)x^2 \frac{\partial g_{Tf}(x)}{\partial x}\Delta\hat{\sigma}_{Dk}^{qg} + D_g(z)x g_{Tf}(x)\Delta\hat{\sigma}_k^{qg}\right], \tag{53}$$

where $\mathcal{S}_k = \sin(\Phi_S - \chi)$ for $k = 1, 2, 3, 4$ and $\mathcal{S}_k = \cos(\Phi_S - \chi)$ for $k = 8, 9$. Note that we may substitute $x\partial g_{Tf}/\partial x \approx -\Delta q_f(x)$ in the above expression. The hard coefficients in the quark-fragmenting (qq) channel are given by

$$\Delta\hat{\sigma}_{D8}^{qq} = \frac{(N_c^2-1)\hat{x}\,\hat{z}}{2N_c^2 Q(1-\hat{z})^2}[(1-\hat{z})(1-\hat{x}+\hat{z}-3\hat{x}\,\hat{z}+N_c^2(1-\hat{x}-\hat{z}+3\hat{x}\,\hat{z}))+2(1-2\hat{x})\hat{z}\log(\hat{z})],$$
$$\Delta\hat{\sigma}_{D9}^{qq} = \frac{(N_c^2-1)(1-\hat{x})\hat{x}\,\hat{z}}{2N_c^2 q_T(1-\hat{z})^2}[(1-\hat{z})(3N_c^2(1-\hat{z})+3\hat{z}-1)-2(1-2\hat{z})\log(\hat{z})], \tag{54}$$

$$\begin{aligned}
\Delta\hat{\sigma}_1^{qq} &= \frac{N_c^2-1}{2N_c^2 q_T(1-\hat{z})\hat{z}}[(1-\hat{z})(\hat{z}\,\hat{x}(\hat{x}(3+10\hat{z})-3(1+\hat{z}))-1)\\
&\quad + N_c^2\hat{z}(\hat{x}^2(3+2\hat{z}(5\hat{z}-6))-1-3\hat{x}(1-\hat{z})^2)+6\hat{x}(2\hat{x}-1)\hat{z}^2\log(\hat{z})],\\
\Delta\hat{\sigma}_2^{qq} &= \frac{(N_c^2-1)\hat{x}}{{N_c}^2 q_T(1-\hat{z})}[(1-\hat{z})((1+N_c^2)(-1+\hat{x})+(N_c^2-1)(1-3\hat{x})\hat{z})+2(2\hat{x}-1)\hat{z}\log(\hat{z})],\\
\Delta\hat{\sigma}_3^{qq} &= \frac{(N_c^2-1)\hat{x}}{4N_c^2 Q(1-\hat{x})(1-\hat{z})^2}[(1-\hat{z})\{(1-\hat{x})(5\hat{x}+N_c^2(2-11\hat{x}))\hat{z}-(1+N_c^2)(1-\hat{x})^2\\
&\quad -(N_c^2-1)(1+\hat{x}(14\hat{x}-13))\hat{z}^2\}-2\hat{z}(1-\hat{z}-\hat{x}(5-4\hat{x}-8(1-\hat{x})\hat{z}))\log(\hat{z})],\\
\Delta\hat{\sigma}_4^{qq} &= \frac{(N_c^2-1)\hat{x}}{2N_c^2 q_T(1-\hat{z})^2}[(1-\hat{z})\{3(1-\hat{z})^2+\hat{x}(-3+(5-4\hat{z})\hat{z})\\
&\quad -N_c^2(1-\hat{z})(2-3\hat{z}+\hat{x}(-2+4\hat{z}))\}-2(\hat{x}-(1-\hat{z})^2-2\hat{x}(1-\hat{z})\hat{z})\log(\hat{z})],\\
\Delta\hat{\sigma}_8^{qq} &= \frac{(N_c^2-1)\hat{x}}{4N_c^2 Q(1-\hat{x})(1-\hat{z})^2}[(1+N_c^2)(1-\hat{x})^2+(1-\hat{x})(5-10\hat{x}+N_c^2(6\hat{x}-5))\hat{z}\\
&\quad -(9+\hat{x}(15\hat{x}-26)-N_c^2(7+9(\hat{x}-2)\hat{x}))\hat{z}^2\\
&\quad -(N_c^2-1)(3+\hat{x}(4\hat{x}-9))\hat{z}^3-2\hat{z}(\hat{x}(7-4\hat{x}-2\hat{z})+\hat{z}-3)\log(\hat{z})],\\
\Delta\hat{\sigma}_9^{qq} &= \frac{(N_c^2-1)\hat{x}}{2N_c^2 q_T(1-\hat{z})^2}[(1-\hat{z})(2N_c^2(1-\hat{x}(1-\hat{z})-2\hat{z})(1-\hat{z})-3+\hat{z}(9-4\hat{z})+\hat{x}(3-(7-2\hat{z})\hat{z}))\\
&\quad -2(1+(\hat{z}-3)\hat{z}+\hat{x}(2\hat{z}-1))\log(\hat{z})],
\end{aligned} \tag{55}$$

and in the gluon-fragmenting (qg) channel by

$$\Delta\hat{\sigma}_{D8}^{qg} = \frac{(N_c^2-1)\hat{x}}{2N_c^2 Q\hat{z}}[\hat{z}(-2+\hat{z}-N_c^2\hat{z}+\hat{x}(4-3\hat{z}+N_c^2(-2+3\hat{z})))-2(1-2\hat{x})(1-\hat{z})\log(1-\hat{z})],$$
$$\Delta\hat{\sigma}_{D9}^{qg} = \frac{(N_c^2-1)(1-\hat{x})\hat{x}(1-\hat{z})}{2{N_c}^2 q_T\hat{z}^2}[\hat{z}(2+3(N_c^2-1)\hat{z})+(2-4\hat{z})\log(1-\hat{z})], \tag{56}$$

$$\begin{aligned}
\Delta\hat{\sigma}_1^{qg} &= \frac{N_c^2-1}{2N_c^2 q_T\hat{z}^2}[\hat{z}(1+\hat{x}^2(-13+23\hat{z}-10\hat{z}^2)+3\hat{x}(2-3\hat{z}+\hat{z}^2))\\
&\quad -N_c^2(1-\hat{z})(-1-3\hat{x}\hat{z}^2+\hat{x}^2(1-8\hat{z}+10\hat{z}^2))-6\hat{x}(-1+2\hat{x})(1-\hat{z})^2\log(1-\hat{z})],\\
\Delta\hat{\sigma}_2^{qg} &= \frac{(N_c^2-1)\hat{x}(1-\hat{z})}{N_c^2 q_T\hat{z}^2}[\hat{z}(2-\hat{z}+N_c^2\hat{z}-\hat{x}(4-3\hat{z}+{N_c}^2(-2+3\hat{z})))+2(1-2\hat{x})(1-\hat{z})\log(1-\hat{z})],\\
\Delta\hat{\sigma}_3^{qg} &= -\frac{(N_c^2-1)\hat{x}}{4{N_c}^2 Q(1-\hat{x})\hat{z}^2}[\hat{z}\{(-1+\hat{z})(2+(N_c^2-1)\hat{z})+\hat{x}(10-24\hat{z}+13\hat{z}^2+N_c^2(-4+16\hat{z}-13\hat{z}^2))\\
&\quad +\hat{x}^2(-8+23\hat{z}-14\hat{z}^2+N_c^2(4-17\hat{z}+14\hat{z}^2))\}\\
&\quad +2(1-\hat{z})(-1+\hat{x}(5-8\hat{z})+\hat{z}+\hat{x}^2(-4+8\hat{z}))\log(1-\hat{z})],\\
\Delta\hat{\sigma}_4^{qg} &= -\frac{(N_c^2-1)\hat{x}(1-\hat{z})}{2{N_c}^2 q_T\hat{z}^3}[\hat{z}(2+(4N_c^2-3)\hat{z}-3(N_c^2-1)\hat{z}^2+\hat{x}(-2+(3-2{N_c}^2)\hat{z}+4(N_c^2-1)\hat{z}^2))\\
&\quad +2((1-\hat{z})^2-\hat{x}(1-2\hat{z}+2\hat{z}^2))\log(1-\hat{z})],
\end{aligned}$$

$$\Delta\hat{\sigma}_8^{qg} = \frac{(N_c^2-1)\hat{x}}{4N_c^2 Q(1-\hat{x})\hat{z}^2}[\hat{z}\{6-(1+N_c{}^2)\hat{z}+3(N_c^2-1)\hat{z}^2+\hat{x}(-22+8\hat{z}+9\hat{z}^2+N_c{}^2(4-9\hat{z}^2))$$
$$+\hat{x}^2(16-9\hat{z}-4\hat{z}^2+N_c^2(-4+3\hat{z}+4\hat{z}^2))\}+2(1-\hat{z})(3+8\hat{x}^2+\hat{z}-\hat{x}(11+2\hat{z}))\log(1-\hat{z})],$$
$$\Delta\hat{\sigma}_9^{qg} = \frac{(N_c^2-1)\hat{x}(1-\hat{z})}{2N_c^2 q_T\hat{z}^3}[\hat{z}((4-N_c^2)\hat{z}-4-4(N_c^2-1)\hat{z}^2+\hat{x}(4+3(N_c^2-2)\hat{z}+2(N_c^2-1)\hat{z}^2))$$
$$+2(-2+2\hat{x}+3\hat{z}-4\hat{x}\,\hat{z}+\hat{z}^2)\log(1-\hat{z})]. \tag{57}$$

Let us briefly comment on the analytic structure of the above results. The hard kernels depend on the virtual quark propagator $1/(p_1-l_1)^2 \approx 1/(-2p_1^+ l_1^-)$. We have parametrized the fragmenting parton momentum as $p_q = p_2 - l_1 = P_h/z$ and $l_1 = P_h/z$ in the $q\to q$ and $q\to g$ channels, respectively. Since $P_h^- = z_f q^-$ and $p_2^- = q^-$, we have $l_1^- = (1-\hat{z})q^-$ in the former case, and $l_1^- = \hat{z}q^-$ in the latter case. This is why the hard cross sections for the $q\to q$ and $q\to g$ channels contain the factor $1/(1-\hat{z})$ and $1/\hat{z}$, respectively. When $z_f \ll 1$, both factors $1/(1-\hat{z}) = z/(z-z_f)$ and $1/\hat{z} = z/z_f$ become large as z is varied between z_f and 1. When $z_f \to 1$, only the former becomes large around the endpoint $z \gtrsim z_f$, so the $q\to q$ channel dominates over the $q\to g$ channel. This observation will be confirmed in the later numerical analysis. The denominator q_T hints that higher-order corrections will introduce the large Sudakov logarithms $\ln^2(Q/q_T)$ at low q_T, whose resummation should be implemented in principle. This is however beyond the scope of this work.

V. COMPUTATION OF THE HARD PART: GLUON INITIATED CHANNEL

The gluon initiated channel is somewhat simpler, since the right diagram in Fig. 2 does not contribute due to Furry's theorem as already pointed out. We thus consider only four diagrams: the left diagram in Fig. 2 and its crossing diagrams with the photon and gluon attachments being interchanged. Considering the quark-fragmenting channel for definiteness, we sum the four diagrams and their complex-conjugates in the form

$$S^{(0)\mu\nu\alpha\beta}(k) = -\frac{ig^4}{2(N_c^2-1)}(2\pi)\delta((k+q-p_q)^2)\int\frac{d^4l_2}{(2\pi)^4}(2\pi)\delta(l_2^2)(2\pi)\delta((p_2-l_2)^2)$$
$$\times[A_{lj}^{\alpha\mu}(k+q-p_q)\bar{M}_{jikl}(k+q-p_q,l_2)A_{ik}^{\nu\beta}(l_2) - A_{lj}^{\beta\nu}(k+q-p_q)\bar{M}_{jikl}(k+q-p_q,l_2)A_{ik}^{\mu\alpha}(l_2)], \tag{58}$$

with

$$\bar{M}_{jikl}(k+q-p_q,l_2) = -\frac{N_c^2-1}{4N_c}\frac{1}{(k+q-p_q-l_2)^2}[\not{p}_q\gamma^\rho(\not{p}_2-\not{l}_2)]_{ji}[\not{l}_2\gamma_\rho(\not{k}+\not{q}-\not{p}_q)]_{kl}, \tag{59}$$

$$A^{\alpha\mu}(k+q-p_q) = \gamma^\alpha\frac{\not{p}_q-\not{q}}{(p_q-q)^2}\gamma^\mu + \gamma^\mu\frac{\not{p}_q-\not{k}}{(p_q-k)^2}\gamma^\alpha, \tag{60}$$

$$A^{\nu\beta}(l_2) = \gamma^\nu\frac{\not{p}_1-\not{l}_2}{(p_1-l_2)^2}\gamma^\beta + \gamma^\beta\frac{\not{q}-\not{l}_2}{(q-l_2)^2}\gamma^\nu. \tag{61}$$

Here k represents the initial gluon momentum, p_q is the observed quark, with the unobserved antiquark carrying the momentum $k+q-p_q$ (equal to $l_1 = p_2 - p_q$ in the collinear limit), and l_2 is the loop momentum. The derivative $\partial/\partial k^\lambda$ in (32) can be performed along the steps analogous to the case of the quark initiated channel. Defining

$$S^{(0)\mu\nu\alpha\beta}(k) = g^4(2\pi)\delta((k+q-p_q)^2)\int\frac{d^2\vec{l}_{2T}}{(2\pi)^3}\frac{dl_2^+}{2l_2^+}(2\pi)\delta((k+q-l_2)^2)\hat{S}^{(0)\mu\nu\alpha\beta}(k), \tag{62}$$

where $\hat{S}^{(0)\mu\nu\alpha\beta}(k)$ can be read off from (58), we find

$$\frac{d^6\Delta\sigma}{dx_B dQ^2 dz_f dq_T^2 d\phi d\chi} = \frac{\alpha_{\rm em}^2\alpha_S^2 M_N}{16\pi^2 x_B^2 S_{ep}^2 Q^2}\sum_k \mathcal{A}_k \int\frac{dx}{x}\int\frac{dz}{z}(2\pi)\delta\left(\frac{q_T^2}{Q^2}-\left(1-\frac{1}{\hat{x}}\right)\left(1-\frac{1}{\hat{z}}\right)\right)\sum_f e_f^2 D_f(z)$$
$$\times 2i\Bigg\{\mathcal{G}_{3T}(x)\int\frac{d^2\vec{l}_{2T}dl_2^+}{(2\pi)^3 2l_2^+}(2\pi)\delta((p_2-l_2)^2)\epsilon^{n\alpha\beta S_T}\hat{S}_\mu^{(0)\alpha'\beta'}(p_1)\omega_{\alpha'\alpha}\omega_{\beta'\beta}\tilde{\mathcal{V}}_k^{\mu\nu}$$
$$+x^2\frac{\partial\mathcal{G}_{3T}(x)}{\partial x}\frac{l_{1T}^\beta\epsilon^{\alpha PnS_T}-l_{1T}^\alpha\epsilon^{\beta PnS_T}}{p_1\cdot l_1}\int\frac{d^2\vec{l}_{2T}dl_2^+}{(2\pi)^3 2l_2^+}(2\pi)\delta((p_2-l_2)^2)\hat{S}_{\mu\nu\alpha\beta}^{(0)}(p_1)\tilde{\mathcal{V}}_k^{\mu\nu}$$
$$+x\mathcal{G}_{3T}(x)\frac{\partial}{\partial x}\Bigg\{x\int\frac{d^2\vec{l}_{2T}dl_2^+}{(2\pi)^3 2l_2^+}(2\pi)\delta((p_2-l_2)^2)$$
$$\times\left[\frac{l_{1T}^\beta\epsilon^{\alpha PnS_T}-l_{1T}^\alpha\epsilon^{\beta PnS_T}}{p_1\cdot l_1}+\frac{l_{2T}^\beta\epsilon^{\alpha PnS_T}-l_{2T}^\alpha\epsilon^{\beta PnS_T}}{p_1\cdot(p_2-l_2)}\right]\hat{S}_{\mu\nu\alpha\beta}^{(0)}(p_1)\tilde{\mathcal{V}}_k^{\mu\nu}\Bigg\}$$
$$-x\mathcal{G}_{3T}(x)\int\frac{d^2\vec{l}_{2T}dl_2^+}{(2\pi)^3 2l_2^+}(2\pi)\delta((p_2-l_2)^2)\frac{l_{2T}^\beta\epsilon^{\alpha PnS_T}-l_{2T}^\alpha\epsilon^{\beta PnS_T}}{p_1\cdot(p_2-l_2)}x\frac{\partial}{\partial x}\hat{S}_{\mu\nu\alpha\beta}^{(0)}(p_1)\tilde{\mathcal{V}}_k^{\mu\nu}$$
$$-x\mathcal{G}_{3T}(x)\int\frac{d^2\vec{l}_{2T}dl_2^+}{(2\pi)^3 2l_2^+}(2\pi)\delta((p_2-l_2)^2)(g_T^{\beta\lambda}\epsilon^{\alpha PnS_T}-g_T^{\alpha\lambda}\epsilon^{\beta PnS_T})\left(\frac{\partial}{\partial k^\lambda}\hat{S}_{\mu\nu\alpha\beta}^{(0)}(k)\right)_{k=p_1}\tilde{\mathcal{V}}_k^{\mu\nu}\Bigg\}. \quad (63)$$

It will be useful to write the 2nd line as

$$\epsilon^{n\alpha\beta S_T}\hat{S}_{\mu\nu}^{(0)\alpha'\beta'}(p_1)\omega_{\alpha'\alpha}\omega_{\beta'\beta} = \epsilon^{nP\beta S_T}\hat{S}_{\mu\nu n\beta}^{(0)}-\epsilon^{nP\alpha S_T}\hat{S}_{\mu\nu\alpha n}^{(0)}. \quad (64)$$

Similar to (45) for the quark-initiated channel, the individual lines in (63) contain infrared divergences which must be canceled in the sum over all the lines. We will prove this cancellation in Appendix B.

The hard coefficients can be obtained in complete analogy to the quark initiated channel. We have the same sets of roots (a_1, a_2) as before [see (46) and (48)]. As we will show in Appendix B, a divergence comes neither from the $p_1 - l_2$ propagator (corresponding to the choice $a_2 = -1$ for the root) nor from the $q - l_2$ propagator (corresponding to the choice $a_2 = 1$) in (61). Therefore, the l_{2T} loop integral is finite, which can be performed analytically. We have also confirmed that, similarly to the previous case, we obtain an expression independent of the choice of the roots for $l_{1(a_1)}^+$ after the loop integral and after the sum over the $l_{2(a_2)}^+$ roots. All in all, the final result for the cross section can be written in a compact way as

$$\frac{d^6\Delta\sigma}{dx_B dQ^2 dz_f dq_T^2 d\phi d\chi} = \frac{\alpha_{\rm em}^2\alpha_S^2 M_N}{16\pi^2 x_B^2 S_{ep}^2 Q^2}\sum_k \mathcal{A}_k\mathcal{S}_k\int_{x_{\min}}^1\frac{dx}{x}\int_{z_{\min}}^1\frac{dz}{z}\delta\left(\frac{q_T^2}{Q^2}-\left(1-\frac{1}{\hat{x}}\right)\left(1-\frac{1}{\hat{z}}\right)\right)$$
$$\times\sum_f e_f^2 D_f(z)\left[x^2\frac{\partial\mathcal{G}_{3T}(x)}{\partial x}\Delta\hat{\sigma}_{Dk}^{qq}+x\mathcal{G}_{3T}(x)\Delta\hat{\sigma}_k^{qq}\right], \quad (65)$$

with $x\partial\mathcal{G}_{3T}/\partial x \approx -\Delta G(x)/2$ in the present approximation. The hard coefficients are given explicitly by

$$\Delta\hat{\sigma}_{D8}^{qq} = \frac{2(1-\hat{x})\hat{x}}{N_c Q(1-\hat{z})^2\hat{z}}[(1-\hat{x})(\hat{z}\log(\hat{z})-(1-\hat{z})\log(1-\hat{z}))+\hat{x}\hat{z}(1-\hat{z})(1-2\hat{z})],$$
$$\Delta\hat{\sigma}_{D9}^{qq} = \frac{2(1-\hat{x})^2\hat{x}}{N_c q_T(1-\hat{z})^2\hat{z}^2}[(1-\hat{z})^2\log(1-\hat{z})+\hat{z}^2\log(\hat{z})+\hat{z}(1-\hat{z})(\hat{z}^2+(1-\hat{z})^2)], \quad (66)$$

$$
\begin{aligned}
\Delta\hat{\sigma}_1^{qq} &= \frac{(1-\hat{x})}{N_c q_T(1-\hat{z})\hat{z}^2}[(1-2\hat{z})(1+2\hat{x}^2(1-2\hat{z})^2-(1-\hat{z})\hat{z}-2\hat{x}(1-(1-\hat{z})\hat{z}))\\
&\quad+6(1-\hat{x})\hat{x}((1-\hat{z})\log(1-\hat{z})-\hat{z}\log(\hat{z}))],\\
\Delta\hat{\sigma}_2^{qq} &= \frac{4(1-\hat{x})\hat{x}}{N_c q_T(1-\hat{z})\hat{z}^2}[(1-\hat{z})(\hat{x}(2\hat{z}-1)\hat{z}+(1-\hat{x})\log(1-\hat{z}))-(1-\hat{x})\hat{z}\log(\hat{z})],\\
\Delta\hat{\sigma}_3^{qq} &= \frac{\hat{x}}{N_c Q(1-\hat{z})^2\hat{z}^2}[(1-\hat{z})\hat{z}(1-2(1-\hat{z})\hat{z}+\hat{x}(-6+(13-12\hat{z})\hat{z})+\hat{x}^2(5-12(1-\hat{z})\hat{z}))\\
&\quad+(1-\hat{x})((1-\hat{z})(1-\hat{z}+\hat{x}(-3+4\hat{z}))\log(1-\hat{z})-\hat{z}(1-\hat{z}-\hat{x}(1-4\hat{z}))\log(\hat{z}))],\\
\Delta\hat{\sigma}_4^{qq} &= \frac{2(1-\hat{x})\hat{x}}{N_c q_T(1-\hat{z})^2\hat{z}^3}[(1-\hat{z})\{\hat{z}(\hat{x}-2\hat{x}\,\hat{z}\,(2+\hat{z}(-3+2\hat{z}))-(1-\hat{z})(1+\hat{z}(-3+4\hat{z})))\\
&\quad-(1-\hat{x}(1-\hat{z}))(1-\hat{z})\log(1-\hat{z})\}-\hat{x}\hat{z}^3\log(\hat{z})],\\
\Delta\hat{\sigma}_8^{qq} &= \frac{\hat{x}}{N_c Q(1-\hat{z})^2\hat{z}^2}[(-1+\hat{z})\hat{z}(-3+10\hat{x}-7\hat{x}^2+(-2+\hat{x})\hat{z}+2(1+2(-1+\hat{x})\hat{x})\hat{z}^2)\\
&\quad+(1-\hat{x})((1-\hat{z})(3-3\hat{z}+\hat{x}(-5+2\hat{z}))\log(1-\hat{z})-\hat{z}(1-3\hat{z}+\hat{x}(-1+2\hat{z}))\log(\hat{z}))],\\
\Delta\hat{\sigma}_9^{qq} &= \frac{-2(1-\hat{x})\hat{x}}{N_c q_T(1-\hat{z})^2\hat{z}^3}[(2+\hat{x}(-2+\hat{z})-2\hat{z})(1-\hat{z})^2\log(1-\hat{z})+\hat{z}^2(1-\hat{x}-(2-\hat{x})\hat{z})\log(\hat{z})\\
&\quad-\hat{z}(1-\hat{z})(-2+3\hat{z}+(-1+\hat{z})(-2\hat{x}+\hat{x}z+2(-1+\hat{x})\hat{z}^2))].
\end{aligned}
\tag{67}
$$

In this computation we have chosen the quark to be observed in the final state ($p_q \to P_h/z$) while the antiquark goes unobserved. As a nontrivial check we have verified that taking the antiquark as the observed final state ($l_1 \to P_h/z$) and the quark as the unobserved one, we recover exactly the same hard coefficients.

VI. NUMERICAL RESULTS

With all the analytical results presented in the previous sections, we are now ready to make predictions for EIC measurements. Specifically, we will numerically compute the asymmetries from the following definition

$$
A_{UT}^{\sin(\alpha\phi_h+\beta\phi_S)} = \frac{2\int_0^{2\pi} d\phi_h d\phi_S \sin(\alpha\phi_h+\beta\phi_S)[d\sigma(\phi_h,\phi_S)-d\sigma(\phi_h,\phi_S+\pi)]}{\int_0^{2\pi} d\phi_h d\phi_S[d\sigma(\phi_h,\phi_S)+d\sigma(\phi_h,\phi_S+\pi)]},
\tag{68}
$$

where $d\sigma(\phi_h,\phi_S)$ is a shorthand for

$$
d\sigma(\phi_h,\phi_S) \equiv \frac{d^6\sigma}{dx_B dQ^2 dz_f dq_T^2 d\phi d\chi}.
\tag{69}
$$

The numerator of (68) is proportional to the $\mathcal{O}(\alpha_s^2)$ polarized cross section we calculated. In terms of the Fourier coefficients (19), we have

$$
\begin{aligned}
\mathcal{F}_1 &= \alpha_S M_N \mathcal{F}_0 \int \frac{dx}{x}\int \frac{dz}{z}\delta\left(\frac{q_T^2}{Q^2}-\left(1-\frac{1}{\hat{x}}\right)\left(1-\frac{1}{\hat{z}}\right)\right)\sum_f e_f^2 \\
&\quad\times[(1+\cosh^2\psi)(D_f(z)xg_{Tf}(x)\Delta\hat{\sigma}_1^{qq}+D_f(z)x\mathcal{G}_{3T}(x)\Delta\hat{\sigma}_1^{qq}+D_g(z)xg_{Tf}(x)\Delta\hat{\sigma}_1^{qg}) \\
&\quad-2(D_f(z)xg_{Tf}(x)\Delta\hat{\sigma}_2^{qq}+D_f(z)x\mathcal{G}_{3T}(x)\Delta\hat{\sigma}_2^{qq}+D_g(z)xg_{Tf}(x)\Delta\hat{\sigma}_2^{qg})], \\
\mathcal{F}_2 &= \alpha_S M_N \mathcal{F}_0 \int \frac{dx}{x}\int \frac{dz}{z}\delta\left(\frac{q_T^2}{Q^2}-\left(1-\frac{1}{\hat{x}}\right)\left(1-\frac{1}{\hat{z}}\right)\right)\sum_f e_f^2(-\sinh 2\psi) \\
&\quad\times[D_f(z)xg_{Tf}(x)\Delta\hat{\sigma}_3^{qq}+D_f(z)x\mathcal{G}_{3T}(x)\Delta\hat{\sigma}_3^{qq}+D_g(z)xg_{Tf}(x)\Delta\hat{\sigma}_3^{qg}], \\
\mathcal{F}_3 &= \alpha_S M_N \mathcal{F}_0 \int \frac{dx}{x}\int \frac{dz}{z}\delta\left(\frac{q_T^2}{Q^2}-\left(1-\frac{1}{\hat{x}}\right)\left(1-\frac{1}{\hat{z}}\right)\right)\sum_f e_f^2\sinh^2\psi \\
&\quad\times[(D_f(z)xg_{Tf}(x)\Delta\hat{\sigma}_4^{qq}+D_f(z)x\mathcal{G}_{3T}(x)\Delta\hat{\sigma}_4^{qq}+D_g(z)xg_{Tf}(x)\Delta\hat{\sigma}_4^{qg})], \\
\mathcal{F}_4 &= \alpha_S M_N \mathcal{F}_0 \int \frac{dx}{x}\int \frac{dz}{z}\delta\left(\frac{q_T^2}{Q^2}-\left(1-\frac{1}{\hat{x}}\right)\left(1-\frac{1}{\hat{z}}\right)\right)\sum_f e_f^2(-\sinh 2\psi) \\
&\quad\times[D_f(z)x^2g'_{Tf}(x)\Delta\hat{\sigma}_{D8}^{qq}+D_f(z)x^2\mathcal{G}'_{3T}(x)(x)\Delta\hat{\sigma}_{D8}^{qq}+D_g(z)x^2g'_{Tf}(x)\Delta\hat{\sigma}_{D8}^{qg} \\
&\quad+D_f(z)xg_{Tf}(x)\Delta\hat{\sigma}_8^{qq}+D_f(z)x\mathcal{G}_{3T}(x)\Delta\hat{\sigma}_8^{qq}+D_g(z)xg_{Tf}(x)\Delta\hat{\sigma}_8^{qg}], \\
\mathcal{F}_5 &= \alpha_S M_N \mathcal{F}_0 \int \frac{dx}{x}\int \frac{dz}{z}\delta\left(\frac{q_T^2}{Q^2}-\left(1-\frac{1}{\hat{x}}\right)\left(1-\frac{1}{\hat{z}}\right)\right)\sum_f e_f^2\sinh^2\psi \\
&\quad\times[D_f(z)x^2g'_{Tf}(x)\Delta\hat{\sigma}_{D9}^{qq}+D_f(z)x^2\mathcal{G}'_{3T}(x)\Delta\hat{\sigma}_{D9}^{qq}+D_g(z)x^2g'_{Tf}(x)\Delta\hat{\sigma}_{D9}^{qg} \\
&\quad+D_f(z)xg_{Tf}(x)\Delta\hat{\sigma}_9^{qq}+D_f(z)x\mathcal{G}_{3T}(x)\Delta\hat{\sigma}_9^{qq}+D_g(z)xg_{Tf}(x)\Delta\hat{\sigma}_9^{qg}],
\end{aligned}
\tag{70}
$$

with the definition

$$
\mathcal{F}_0 = \frac{\alpha_{\rm em}^2\alpha_S}{16\pi^2x_B^2S_{ep}^2Q^2}, \tag{71}
$$

and the abbreviations

$$
xg'_{Tf}(x) \equiv x\frac{\partial g_{Tf}(x)}{\partial x} \approx -\Delta q_f(x), \qquad x\mathcal{G}'_{3T}(x) \equiv x\frac{\partial \mathcal{G}_{3T}(x)}{\partial x} \approx -\frac{\Delta G(x)}{2}. \tag{72}
$$

The integration variables x and z are in the ranges

$$
1 > x > x_{\rm min} \equiv x_B\left(1+\frac{z_f}{1-z_f}\frac{q_T^2}{Q^2}\right), \qquad 1 > z > z_{\rm min} \equiv z_f\left(1+\frac{x_B}{1-x_B}\frac{q_T^2}{Q^2}\right). \tag{73}
$$

As for the unpolarized cross section in the denominator, we use the leading-order $\mathcal{O}(\alpha_s)$ formula [17], summarized by Eqs. (54)–(59) in [19]. The angular decomposition can be cast in the following form

$$
\frac{d^6\sigma}{dx_B dQ^2 dz_f dq_T^2 d\phi d\chi} = F^1 + F^{\cos\phi_h}\cos\phi_h + F^{\cos 2\phi_h}\cos 2\phi_h, \tag{74}
$$

Since we integrate over the lepton angle (see below), only the first term F^1 is relevant with the explicit expression

$$F^1 = \mathcal{F}_0 \int \frac{dx}{x} \int \frac{dz}{z} \delta\left(\frac{q_T^2}{Q^2} - \left(1-\frac{1}{\hat{x}}\right)\left(1-\frac{1}{\hat{z}}\right)\right)$$
$$\times \sum_f e_f^2 \{D_f(z) q_f(x)[(1+\cosh^2\psi)\hat{\sigma}_1^{qq} - 2\hat{\sigma}_2^{qq}] + D_g(z) q_f(x)[(1+\cosh^2\psi)\hat{\sigma}_1^{qg} - 2\hat{\sigma}_2^{qg}]$$
$$+ D_f(z) G(x)[(1+\cosh^2\psi)\hat{\sigma}_1^{gq} - 2\hat{\sigma}_2^{gq}]\}, \tag{75}$$

where $G(x)$ is the unpolarized gluon PDF and the summation over f includes both quarks and antiquarks. The hard factors are given by

$$\hat{\sigma}_1^{qq} = \frac{N_c^2-1}{N_c} \hat{x}\,\hat{z} \left\{\frac{1}{Q^2 q_T^2}\left[\frac{Q^4}{\hat{x}^2\hat{z}^2} + (Q^2 - q_T^2)^2\right] + 6\right\},$$
$$\hat{\sigma}_2^{qq} = 2\hat{\sigma}_4^{qq} = 4\frac{N_c^2-1}{N_c}\hat{x}\,\hat{z}, \tag{76}$$

$$\hat{\sigma}_1^{qg} = \frac{N_c^2-1}{N_c}\hat{x}(1-\hat{z})\left\{\frac{1}{Q^2 q_T^2}\left[\frac{Q^4}{\hat{x}^2\hat{z}^2} + \frac{(1-\hat{z}^2)}{\hat{z}^2}\left(Q^2 - \frac{\hat{z}^2}{(1-\hat{z})^2} q_T^2\right)^2\right] + 6\right\},$$
$$\hat{\sigma}_2^{qg} = 2\hat{\sigma}_4^{qg} = 4\frac{N_c^2-1}{N_c}\hat{x}(1-\hat{z}), \tag{77}$$

$$\hat{\sigma}_1^{gq} = \hat{x}(1-\hat{x})\left[\frac{Q^2}{q_T^2}\left(\frac{1}{\hat{x}^2\hat{z}^2} - \frac{2}{\hat{x}\,z} + 2\right) + 10 - \frac{2}{\hat{x}} - \frac{2}{\hat{z}}\right],$$
$$\hat{\sigma}_2^{gq} = 2\hat{\sigma}_4^{gq} = 8\hat{x}(1-\hat{x}). \tag{78}$$

Using F^1 (75) and the relation (20), we obtain from (68)

$$A_{UT}^{\sin(\alpha\phi_h+\beta\phi_S)} = \frac{F^{\sin(\alpha\phi_h+\beta\phi_S)}}{F^1}. \tag{79}$$

In practice, we show our results as functions of P_{hT}, z_f or x_B by integrating out all the other variables in the numerator and denominator. Instead of Q^2, it is convenient to use $y = Q^2/(x_B S_{ep})$ so that we have $dQ^2 = x_B S_{ep} dy$ and the relations

$$1 + \cosh^2\psi = 2\frac{1+(1-y)^2}{y^2},$$
$$\sinh^2\psi = 4\frac{1-y}{y^2},$$
$$\sinh 2\psi = 4\frac{(2-y)\sqrt{1-y}}{y^2}. \tag{80}$$

There are general kinematical constraints on the integration ranges of x_B, z_f and y. The condition $x_{\min} < 1$ [see (73)] leads to

$$x_B \le 1 - \frac{1}{z_f(1-z_f)}\frac{P_{hT}^2}{y S_{ep}}. \tag{81}$$

Requiring the upper bound of x_B to be positive, we find a condition on y,

$$y > \frac{1}{z_f(1-z_f)}\frac{P_{hT}^2}{S_{ep}}. \tag{82}$$

Similar constraints can be obtained from $z_{\min} < 1$, which are however not very restrictive because $P_{hT}^2 \ll S_{ep}$. In actual experiments, A_{UT} is integrated over conveniently chosen bins in x_B, z_f and y, and we will follow suit.

Since we are using the leading-order cross sections for both the numerator and denominator, one may ask a legitimate question about the effect of higher order corrections, in particular when $P_{hT} \ll Q$ and the resummation of the Sudakov logarithms is required. While such a procedure is well established for unpolarized cross sections, that for transversely polarized cross sections is poorly understood. On a general ground, we expect that the impact of resummation largely cancels in the ratio, but this has to be checked, and will be left for a future work. As for the scale μ of the QCD coupling constant α_S (and also of PDFs and FFs), we argue that the lower scale $\mu = P_{hT}$ is more appropriate than the larger one $\mu = Q$ in the typical kinematic region $P_{hT} \ll Q$ we are considering. This is understood simply from the aspect of the Sudakov (k_T) resummation usually done in the Fourier conjugate impact parameter space b_T. The running of the coupling tends to pick up a dominant contribution from the large b_T region under the inverse Fourier transformation (for which some prescription is needed to avoid the Landau pole [26]).

Therefore, the choice of a lower scale $\mu = P_{hT} \sim O(1/b_T)$ fits the above all-order picture better.

The computation is performed with the most recent NNPDF and JAM global fits. For the NNPDF sets we use the helicity PDFs from [27] and FFs from [28]. For the JAM sets we use the helicity PDFs and FFs from a simulatenous fit in [29]. $g_{Tf}(x)$ and $\mathcal{G}_{3T}(x)$ are deduced from the helicity PDFs according to the formulas (25) and (30) in the WW approximation. The uncertainties in PDFs (FFs) in NNPDF and JAM fits are quantified by the Monte Carlo replica method to generate a variance according to the normal distribution. In all the plots below the band represents a combination of 1-σ uncertainty due to the replica method and also uncertainty in the scale choice according to $0.5 < \mu/P_{hT} < 2.0$, added in quadrature. Note that the edge $\mu = 0.5P_{hT}$ starts at $P_{hT} = 2$ GeV.

A. Calculation for COMPASS kinematics

Though our approach is most naturally and legitimately applied to the kinematics for EIC, let us first present the results relevant to the COMPASS experiment [15]. Admittedly, the collinear factorization may not be applicable to the COMPASS kinematics since most of the data points have P_{hT} below 1 GeV. There is, however, one published data point with $P_{hT} \approx 1.5$ GeV. We thus only show the P_{hT} distribution for $P_{hT} > 1$ GeV, integrating out the other variables over the following coverage [15]

$$0.003 \le x_B \le 0.7, \qquad 0.1 \le y \le 0.9, \qquad 0.2 \le z_f \le 1, \tag{83}$$

as well as

$$Q^2 > 1\ \text{GeV}^2, \qquad W^2 > 25\ \text{GeV}^2, \tag{84}$$

where $W^2 = (q+P)^2 = Q^2(1-x_B)/x_B$. With a 160 GeV muon beam colliding on a fixed proton target, the center of mass energy is $\sqrt{S_{\mu p}} \approx 17.4$ GeV. The P_{hT} distributions are shown in Fig. 3 for both π^+ and π^- productions.

We see that the Sivers asymmetry for π^+ is smaller than 0.5% in magnitude using the NNPDF fits and about $\sim$0.5% – 1% in magnitude using the JAM fits. In either case, the sign is opposite to the highest P_{hT} COMPASS data point (see the top-right plot in Fig. 9 of [15]). Although the significant experimental uncertainty makes a meaningful comparison difficult, the result does indicate the importance of other sources of SSA, such as the ETQS function. However, $P_{hT} \gtrsim 1$ GeV is the borderline between the collinear and TMD approaches. Therefore, our analysis implies that not only the Sivers function but also the new higher-twist contributions found in [1] need to be included in the global determination of nonperturbative inputs in this regime. As for the Collins asymmetry, our result is negligibly small. The data show nonvanishing central values at $P_{hT} = 1.5$ GeV (see the top-right plot in Fig. 6 of [15]), but they are consistent with zero after the large error bars are taken into account.

B. Calculation for EIC kinematics

We now present our results for the EIC kinematics. Figure 4 shows the z_f distribution of the π^+ Sivers

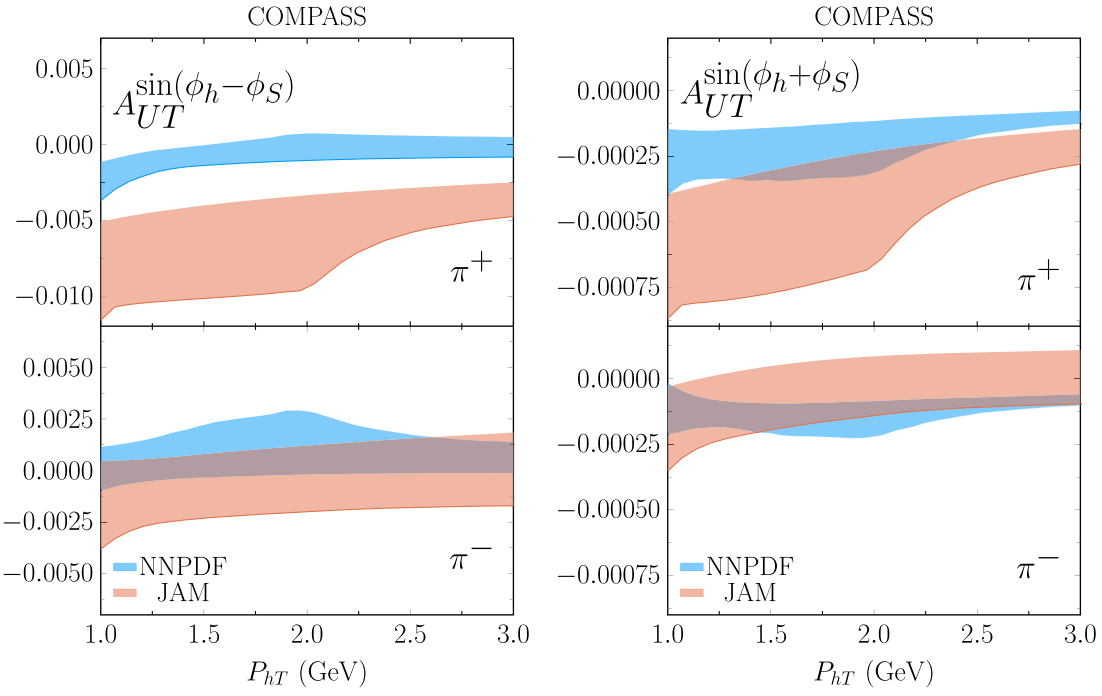

FIG. 3. P_{hT} distributions of Sivers (left) and Collins (right) asymmetries for $\pi^\pm$ production at COMPASS.

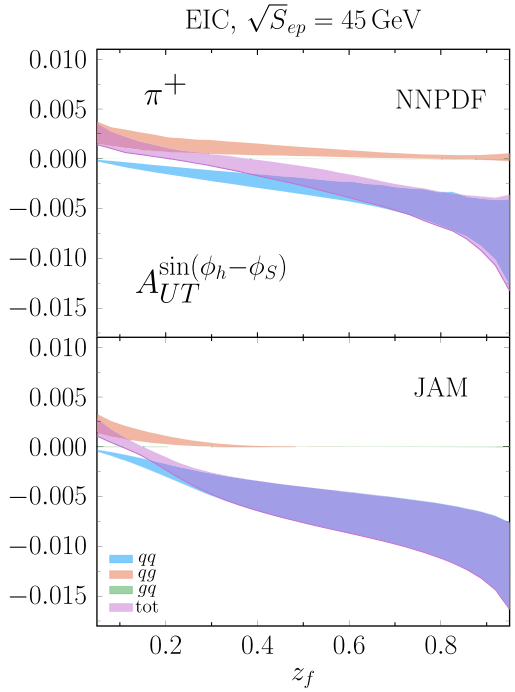

FIG. 4. z_f distributions of the Sivers asymmetry for π^+ production at $\sqrt{S_{ep}} = 45$ GeV differentiated among individual channels.

asymmetry for $\sqrt{S_{ep}} = 45$ GeV integrated over the window $0.1 < x_B < 0.9$ and $0.01 < y < 0.95$ and $P_{hT} > 1$ GeV. The upper bound for the integral over P_{hT} is obtained from (81) by placing the remaining kinematic variables at their extremal values in the above kinematic window. We also impose the conditions $Q^2 > 1\ \mathrm{GeV}^2$ and $W^2 = (P+q)^2 > 25\ \mathrm{GeV}^2$. In addition to the total asymmetry ("tot"), respective contributions from different channels (qq, qg, gq) are shown. The asymmetry is largest in the forward region $z_f \to 1$, at most 1.5% in magnitude, and decreases toward zero as z_f decreases. As we discussed at the end of Sec. IV, the large z_f region is dominated by the quark-fragmenting channel, while the gluon-fragmenting channel becomes important at small z_f. Since the final state quark and gluon are back-to-back, this explains the sign change for the two channels. A somewhat larger asymmetry is observed from the JAM fit than from the NNPDF fit. This is in fact a general feature seen also for example in Fig. 3, but most directly understood from the z_f-distributions in Fig. 4 where the qg channel contribution is dying off more rapidly as $z_f \to 1$ for the JAM fits. Consequently, the cancellation between the qq and the qg channels is less effective using the JAM fits. The underlying reason is the smaller $g \to \pi^+$ FF in the JAM fit than in the NNPDF fit.

Figure 5 gives the P_{hT} distributions of the π^+ Sivers asymmetry in low z_f $(0.05 < z_f < 0.4$, left) and high z_f $(0.5 < z_f < 0.9$, right) bins. We can again see the role of the $g \to \pi^+$ FF: at low z_f the Sivers asymmetry can even become positive (albeit rather small in magnitude) using the NNPDF fits, while in the large z_f region the qg channel quickly dies off so the JAM fits predict a larger (negative) Sivers asymmetry, around $0.5\% \sim 1.5\%$ in magnitude.

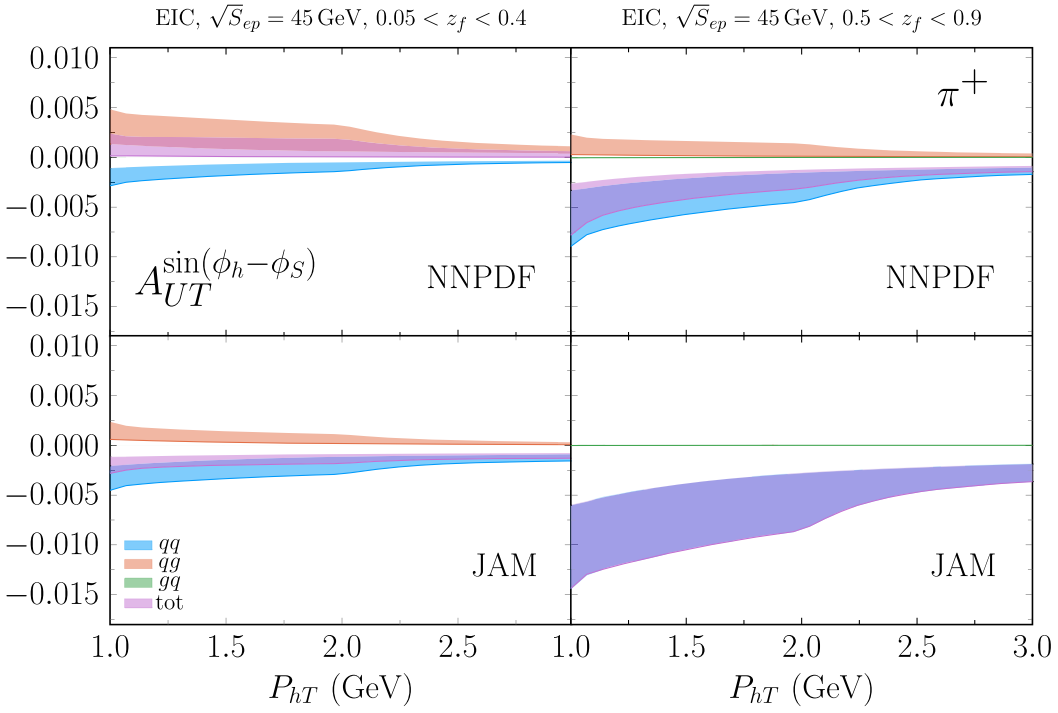

FIG. 5. P_{hT} distributions of the Sivers asymmetry for π^+ production at $\sqrt{S_{ep}} = 45$ GeV in low z_f (left) and high z_f (right) bins.

Note that the gluon-initiated (gq) channel is negligibly small, almost invisible in the plots. A closer look reveals that the contribution to A_N from this channel is less than 10^{-3} in all the bins we have studied. We have anticipated that the gluon-initiated channel gives a small contribution to light-hadron production. However, the suppression is stronger than expected, and we attempt to explain the reason in the concluding section.

Further predictions for the P_{hT} distributions of the π^+ Sivers asymmetry across three bins in x_B and Q^2, using the NNPDF and JAM fits, are exhibited in Fig. 6. We find that the Sivers asymmetry can reach up to 2% in magnitude for the JAM fit covering both large x_B ($0.1 < x_B < 0.7$) and moderate x_B ($0.05 < x_B < 0.1$) bins for the lowest Q^2 bin. Going from moderate to small x_B, the Sivers asymmetry drops to a sub-percent level, as seen in the last x_B bin with $0.001 < x_B < 0.05$. This suppression at small x_B in fact has the same origin as the smallness of the gluon-initiated channel mentioned above (see the discussion in the concluding section). Figure 7 covers the Sivers asymmetry for two collision energies (S_{ep}) and two bins in x_B. The results show very mild dropping of the Sivers asymmetry as $\sqrt{S_{ep}}$ is increased from 45 GeV to the top EIC energy of 140 GeV (see also [30]). The reason is that the energy dependence mainly comes from the y dependence, which roughly cancels out between the numerator and denominator. Compared with an earlier prediction for EIC in the TMD framework at low momentum $P_{hT} < 1$ GeV (see Fig. 21 of [31]), our result for the Sivers asymmetry is similar or somewhat smaller in magnitude but opposite in sign, although a detailed comparison is not possible because there is no overlap in the plotted P_{hT} ranges. This suggests that there are cancellations between different mechanisms which may lead to a sign change. However, we emphasize again that when $P_{hT} \lesssim 1$ GeV, other sources of asymmetries from various twist-three TMDs found in [1] should be added to the contribution from the Sivers function.

Finally, in Fig. 8, we present a full set of moments introduced in (20) and (79) for three different bins in x_B and for fixed bins in Q^2 and z_f ($1 < Q^2 < 10$ GeV^2, $0.5 < z_f < 0.9$). We find that two additional moments $A_{UT}^{\sin(\phi_S)}$ and $A_{UT}^{\sin(2\phi_h-\phi_S)}$ reach up to 2% in magnitude in the highest x_B bin $0.7 < x_B < 0.1$. In the TMD framework for low P_{hT}, the $\sin(\phi_S)$ and $\sin(2\phi_h - \phi_S)$ asymmetries are known to be generated by various twist-three TMDs [32]. We have just demonstrated that the g_T distribution (or its TMD counterpart g_{1T} by extension) is also a potentially significant source of these asymmetries. Indeed, our prediction 1%-2% at $P_{hT} = 1$ GeV is comparable to previous TMD-based calculations [33,34].

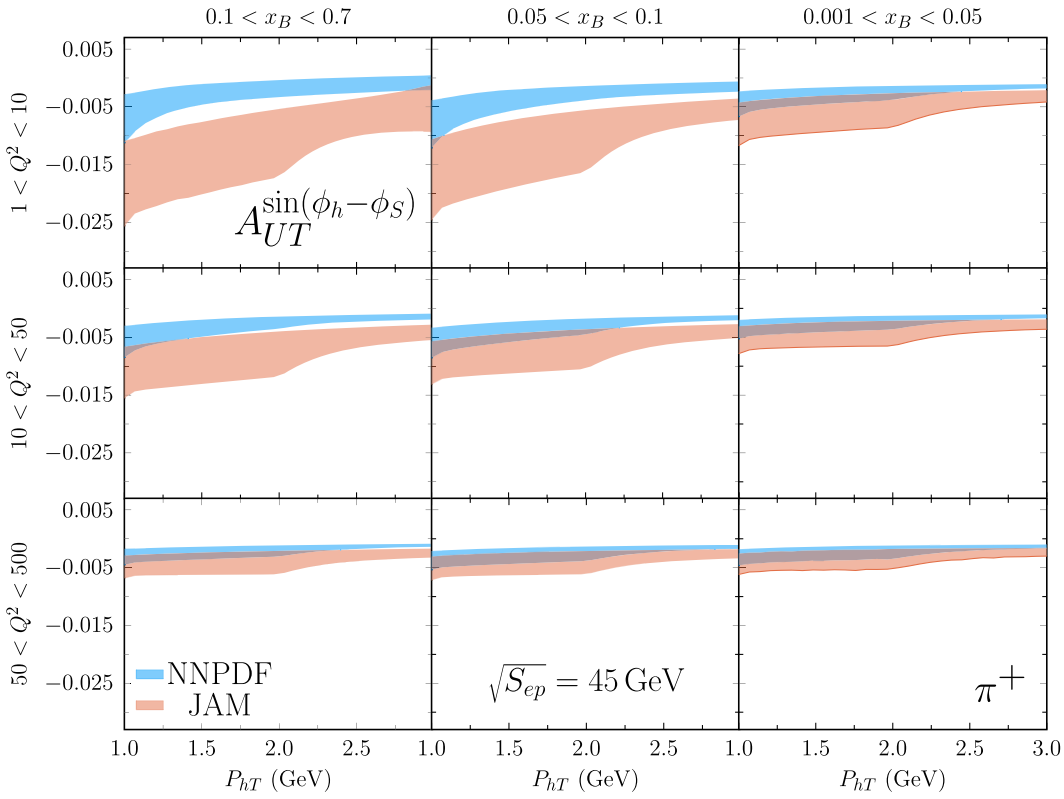

FIG. 6. P_{hT} distributions of the Sivers asymmetry for π^+ production at $\sqrt{S_{ep}} = 45$ GeV for three different x_B and Q^2 bins (we have dropped the units in GeV^2 on the plot), covering $0.5 < z_f < 0.9$.

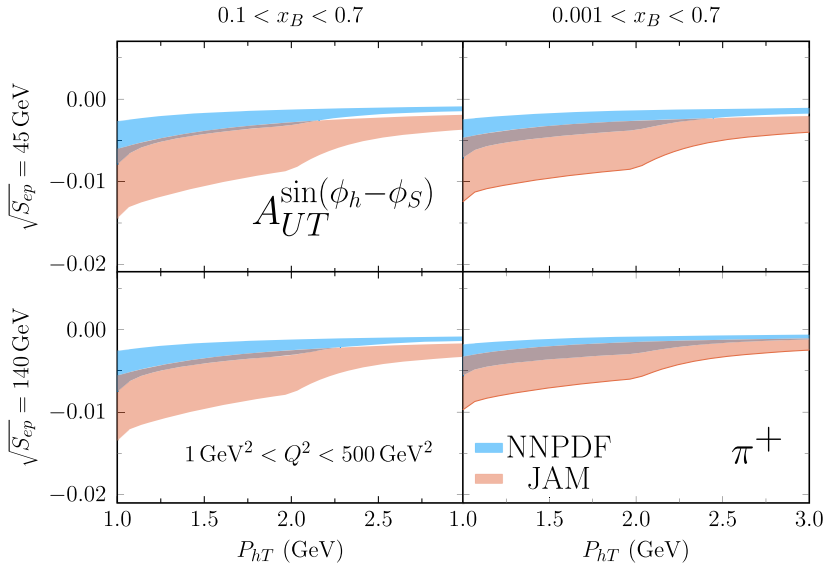

FIG. 7. P_{hT} distributions of the Sivers asymmetry for π^+ production at $\sqrt{S_{ep}} = 45$ GeV and $\sqrt{S_{ep}} = 140$ GeV for two different x_B and for $1 < Q^2 < 500$ GeV^2, covering $0.5 < z_f < 0.9$.

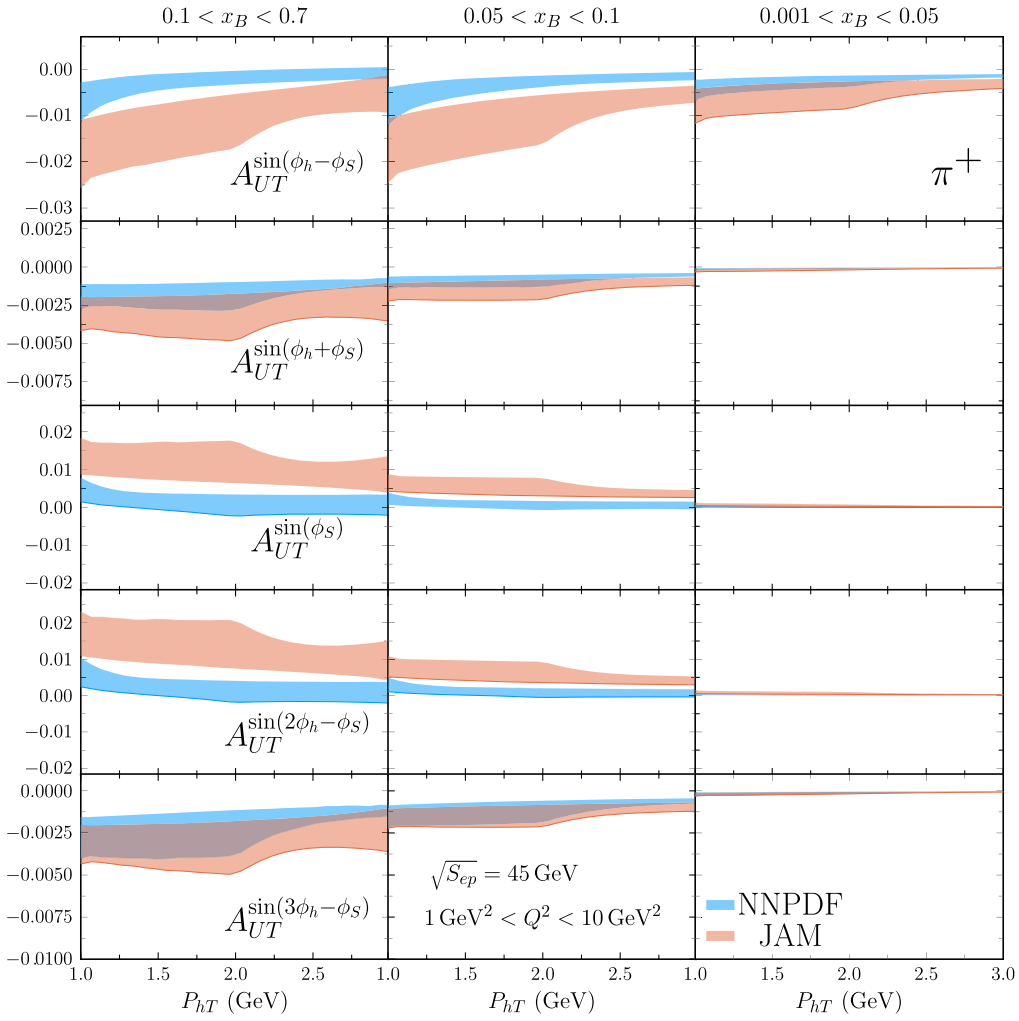

FIG. 8. P_{hT} distributions of all asymmetry moments A_{UT} for π^+ production at $\sqrt{S_{ep}} = 45$ GeV for three different x_B bins integrated over $1 < Q^2 < 10$ GeV^2 and $0.5 < z_f < 0.9$.

VII. DISCUSSIONS AND CONCLUSIONS

In this paper we have performed the complete analytical and numerical evaluation of the novel two-loop contributions to SSA proportional to the twist-two polarized PDFs $\Delta q(x)$ and $\Delta G(x)$. Our results indicate that, at the EIC, A_{UT} for pions can reach 1-2% for the three harmonics $\sin(\phi_h - \phi_S)$, $\sin(\phi_h)$ and $\sin(2\phi_h - \phi_S)$. On the other hand, contributions from the gluon-initiated channel are negligibly small. Since we are dealing with higher-order perturbative diagrams, we have anticipated that the resulting asymmetry would be small. However, the stronger-than-expected suppression we observed, especially in the gluon sector, calls for an explanation. Parametrically, the asymmetry behaves as

$$A_{UT} = \frac{d\Delta\sigma}{d\sigma} \sim \frac{\alpha_s^2 \frac{M_N}{P_{hT}} (x\Delta q(x) \text{ or } x\Delta G(x))}{\alpha_s (q(x) \text{ or } G(x))}. \quad (85)$$

In addition to the obvious factor of α_s, A_{UT} is suppressed by the smallness of polarized PDFs as compared to unpolarized ones. In particular, the gluon-initiated channel is expected to be important for $x \ll 1$, but there, $\Delta G(x) \sim xG(x)$ as a rule of thumb. On top of this, there is a somewhat unexpected extra factor of x in the numerator which comes from the rewriting $\int dx g_T(x) = \int \frac{dx}{x} x g_T(x)$ and $\int dx \mathcal{G}_{3T}(x) = \int \frac{dx}{x} x \mathcal{G}_{3T}(x)$. Of course the same factor exists in the unpolarized cross section in the denominator, which is, however, accompanied by P^+, and the product $xP^+ = p_1^+$ goes into the hard part and gets absorbed. Therefore, our new contribution, especially in the gluon initiated channel, is strongly suppressed like $\sim x^2$ at low x, or in more practical terms, as the selected kinematic bin is sensitive to the low x_B region. This tendency has been clearly shown in Fig. 8. In the literature, gluon-initiated channels are usually ignored in the calculation of A_{UT} for light-hadrons (see, however, an attempt in pp collisions [35]), partly because it is believed to be small, but also because nothing is known about the strength of the three-gluon correlators $\langle FgFF \rangle$. For the first time, we have presented a reliably calculable piece of the gluon initiated contributions, and found very small values. After all, our main interest in the gluon initiated processes focuses on A_{UT} in heavy systems such as open charm and J/ψ. This will be studied elsewhere.

It is worthwhile to compare (85) with the well-known parametric estimate of SSA

$$A_{UT} \sim \frac{\alpha_s m_q}{P_{hT}}, \quad (86)$$

where $m_q \sim$ a few MeV is the current quark mass. This formula has been inferred from the argument in [36], and is often quoted in order to emphasize the smallness of SSA in perturbation theory and the necessity to introduce new nonperturbative distributions. The factor of α_s is because one needs loop diagrams such as in Fig. 1 to get an imaginary part, and the factor of m_q is because one needs a helicity flip. However, this suppression by m_q is illusory for the proton initial state. As is clear from the definitions of g_T and $\mathcal{G}_{3T}$ in (23) and (29), m_q is replaced by the proton mass M_N (see also a related argument in [37]). Thus the correct argument in the DIS case would be that, naively $A_{UT} \sim \frac{\alpha_s M_N}{P_{hT}}$ is large, but the coefficient is suppressed due to the above-mentioned factor x^2, resulting in SSA of about 1% as we have shown. In SIDIS at $P_{hT} > 1$ GeV, this should be comparable to other nonperturbative origins of SSA.

Precisely measuring A_{UT} in the sub-percent region is challenging at the EIC. Conversely, if the future data on A_{UT} turn out to be consistently larger than 1%, most likely genuine twist-three effects are at work. But our result must be subtracted when one tries to extract various twist-three distributions. The distinct kinematical features of our contribution, such as the suppression in low z_f and low-x_B regions, may be useful to isolate this purely perturbative "background." At lower $P_{hT} < 1$ GeV, predictions based on the Sivers function are available [30,31]. However, in the TMD regime $P_{hT} < 1$ GeV, there are many other sources of the $\sin(\phi_h - \phi_S)$ asymmetry which are unrelated to the Sivers function [1], that must be taken into consideration in order to reliably extract the Sivers function.

ACKNOWLEDGMENTS

We thank Shinsuke Yoshida for useful discussions. S. B. would like to thank for the warm hospitality of the Yukawa Institute for Theoretical Physics, Kyoto University where part of this work was performed for which S. B. was supported by the JSPS postdoctoral fellowship for foreign researchers under Grant No. 17F117323. S. B. and A. K. are supported by the Croatian Science Foundation (HRZZ) No. 5332 (UIP-2019-04). The work by Y. H. is supported by the U.S. Department of Energy, Office of Science, Office of Nuclear Physics, under Contract No. DE-SC0012704, and also by Laboratory Directed Research and Development (LDRD) funds from Brookhaven Science Associates. H.-n. L. is supported by the Ministry of Science and Technology of R.O.C. under Grant No. MOST-110-2811-M-001-540-MY3.

APPENDIX A: ANALYSIS OF INFRARED DIVERGENCES: QUARK-INITIATED CHANNEL

In this Appendix we show that the collinear divergences from the l_{2T} integral in (44) cancel. The key step is to establish the QCD Ward identity associated with the l_2 gluon, which is formulated by substituting l_2^β for $A^{\nu\beta}(l_2)$ in $S^{(0)}_{\mu\nu}(k)$. As explained in [1], the part of the cross section, which is contracted with the component l_2^+, is the only piece contributing in the collinear region of l_2. Once the

Ward identity holds, this part of the cross section with the potential divergences must vanish in the collinear limit $l_2^-, l_{2T} \to 0$. Below we demonstrate the cancellation of the collinear divergences by means of the Ward identity. It has been proved in [1] that $\not{k} S^{(0)}_{\mu\nu}(k)$ satisfies the Ward identity, as the momenta p_q, l_1, l_2 and $p_2 - l_2$ are on-shell. The identity should be still valid even when the derivatives apply as in (44). Nevertheless, we will verify the identity explicitly for rigorousness, starting from (44).

The second line in (44), for which

$$l_2^\beta \not{p}_1 \bar{M}^\mu_\beta = 0, \tag{A1}$$

with the notation $\bar{M}^\mu_\beta \equiv A^{\alpha\mu}\bar{M}_{\alpha\beta}$ holds trivially due to on-sell l_1 and $p_2 - l_2$, obeys the Ward identity by itself. In the third line, $l_1 = k + q - p_q$ is not on-shell, and in the fourth and fifth lines, $p_2 - l_2 = k + q - l_2$ is not either prior to taking the derivatives. A generalization of the Ward identity for our discussion, that covers these two cases, is expressed as

$$l_2^\beta \not{k} \bar{M}^\mu_\beta = \frac{N_c(N_c^2-1)}{4} \not{k} A^{\alpha\mu} \not{p}_q \left\{ \frac{(k+q-p_q)^2}{(k+q-p_q-l_2)^2} \gamma_\alpha (\not{k} + \not{q} - \not{l}_2) - \left[\frac{l_{2\alpha}}{(k+q-p_q-l_2)^2} + \frac{N_c^2-1}{N_c^2} \gamma_\alpha \frac{\not{k}+\not{q}}{(k+q)^2} \right] (k+q-l_2)^2 \right\}. \tag{A2}$$

For the third line in (44) with off-shell l_1, (A2) gives

$$l_2^\beta \not{p}_1 \bar{M}^\mu_\beta = \not{p}_1 A^{\alpha\mu} \not{p}_q \frac{N_c(N_c^2-1)}{4} \left[\frac{(p_2-p_q)^2 \gamma_\alpha}{(p_2-p_q-l_2)^2} \right] (\not{p}_2 - \not{l}_2). \tag{A3}$$

We take the derivative $\partial/\partial x$, and then take l_1 on-shell, for which only the derivative of l_1^2 is needed,

$$x \frac{\partial}{\partial x} l_1^2 = x \frac{\partial}{\partial x} (p_2 - p_q)^2 = p_1^\alpha \frac{\partial}{\partial p_1^\alpha} (p_2 - p_q)^2 = 2 p_1 \cdot (p_2 - p_q). \tag{A4}$$

Multiplying (A3) by the prefactor in the third line, we find a nonzero result

$$-\left[\frac{l_1 \cdot S_T}{p_1 \cdot l_1} + \frac{l_2 \cdot S_T}{p_1 \cdot (p_2 - l_2)} \right] x \frac{\partial}{\partial x} (l_2^\beta \not{p}_1 \bar{M}^\mu_\beta) = -\left[l_1 \cdot S_T + \frac{(l_2 \cdot S_T)(p_1 \cdot l_1)}{p_1 \cdot (p_2 - l_2)} \right] \times \not{p}_1 A^{\alpha\mu} (\not{p}_2 - \not{l}_1) \frac{N_c(N_c^2-1)}{2} \frac{\gamma_\alpha}{(l_1 - l_2)^2} (\not{p}_2 - \not{l}_2). \tag{A5}$$

For the fourth line, we first perform the x-derivative and put $p_2 - l_2$ on shell next. In practice, it means that l_2 is independent of x, so the only x dependence stems from p_1. We then write $x\partial/\partial x = p_1^\alpha \partial/\partial p_1^\alpha$ as in (A4), and get

$$\frac{l_2 \cdot S_T}{p_1 \cdot (p_2 - l_2)} x \frac{\partial}{\partial x} (l_2^\beta \not{p}_1 \bar{M}^\mu_\beta) = \frac{(l_2 \cdot S_T)(p_1 \cdot l_1)}{p_1 \cdot (p_2 - l_2)} \not{p}_1 A^{\alpha\mu} (\not{p}_2 - \not{l}_1) \frac{N_c(N_c^2-1)}{2} \frac{\gamma_\alpha}{(l_1 - l_2)^2} (\not{p}_2 - \not{l}_2) - (l_2 \cdot S_T) \not{p}_1 A^{\alpha\mu} (\not{p}_2 - \not{l}_1) \frac{N_c(N_c^2-1)}{2} \left[\frac{l_{2\alpha}}{(l_1 - l_2)^2} + \frac{N_c^2-1}{N_c^2} \gamma_\alpha \frac{\not{p}_2}{p_2^2} \right]. \tag{A6}$$

The fifth line contains

$$S_T^\alpha \left[\frac{\partial}{\partial k_T^\alpha} (l_2^\beta \not{k} \bar{M}^\mu_\beta) \right]_{k=p_1} = (l_1 \cdot S_T) \not{p}_1 A^{\alpha\mu} (\not{p}_2 - \not{l}_1) \frac{N_c(N_c^2-1)}{2} \frac{\gamma_\alpha}{(l_1 - l_2)^2} (\not{p}_2 - \not{l}_2) + (l_2 \cdot S_T) \not{p}_1 A^{\alpha\mu} (\not{p}_2 - \not{l}_1) \frac{N_c(N_c^2-1)}{2} \left[\frac{l_{2\alpha}}{(l_1 - l_2)^2} + \frac{N_c^2-1}{N_c^2} \gamma_\alpha \frac{\not{p}_2}{p_2^2} \right]. \tag{A7}$$

Summing up (A5), (A6) and (A7), we obtain the vanishing net result. Therefore, even though the individual lines in (44) yield nonzero pieces, the QCD Ward identity is respected by their sum.

Next we analyze the collinear divergences in the l_{2T} integral. It has been known in [1] that no infrared divergences arise from the $l_1 - l_2$ and $p_2 - l_1 - l_2$ propagators in (35). The divergence from the $l_1 - l_2$ propagator would appear when

$\vec{l}_{2T} \to \vec{l}_{1T}$, but is canceled in the symmetric piece of $S^{(0)}_{\mu\nu}$. The potential divergence from the $p_2 - l_1 - l_2$ propagator as $\vec{l}_{2T} \to -\vec{l}_{1T}$ is suppressed by the numerator of the respective quark propagator. We thus devote the remainder of this Appendix to the possible divergence from the $p_1 - l_2$ propagator, whose denominator $(p_1 - l_2)^2 = -2p_1^+ l_2^-$ diminishes as $l_{2T} \to 0$ [corresponding to the sign $a_2 = +1$ in (48)]. In this limit $l_2^- = l_{2T}^2/2l_2^+ \to 0$, while the on-shell condition $(p_2 - l_2)^2 = 0$ requires $l_2^+ \to p_2^+$.

We rewrite the Ward identity (A1) as

$$\not{p}_1 \bar{M}^\mu_+ = -\not{p}_1 \frac{l_2^-}{l_2^+} \bar{M}^\mu_- - \not{p}_1 \frac{l_2^i}{l_2^+} \bar{M}^\mu_i, \tag{A8}$$

and examine whether the resultant piece in the second line of (44)

$$\begin{aligned} \mathrm{Tr}\left[\gamma_5 \not{p}_1 \bar{M}^\mu_\beta \gamma^\nu \frac{\not{p}_1 - \not{l}_2}{(p_1 - l_2)^2} \gamma^\beta\right] &= \mathrm{Tr}\left[\gamma_5 \not{p}_1 \bar{M}^\mu_- \gamma^\nu \frac{\not{p}_1 - \not{l}_2}{(p_1 - l_2)^2} \left(-\frac{l_2^-}{l_2^+}\gamma^+ + \gamma^-\right)\right] \\ &\quad + \mathrm{Tr}\left[\gamma_5 \not{p}_1 \bar{M}^\mu_i \gamma^\nu \frac{\not{p}_1 - \not{l}_2}{(p_1 - l_2)^2} \left(-\frac{l_2^i}{l_2^+}\gamma^+ + \gamma^i\right)\right], \end{aligned} \tag{A9}$$

is divergent. Given the denominator in the above expression $(p_1 - l_2)^2 = -2p_1^+ l_2^- \sim O(l_{2T}^2)$ as $l_{2T} \to 0$, the integral will be finite, if the numerator is $O(l_{2T})$. The first term in the numerator, proportional to $l_2^- \gamma^+$, is counted as $l_2^- \sim O(l_{2T}^2)$. The second term, proportional to γ^-, vanishes because of $\gamma^- \not{p}_1 = 0$. The third term, proportional to $l_2^i \gamma^+$, is $O(l_{2T})$ apparently. The fourth term, proportional to γ^i, is at least $O(l_{2T})$ since $\not{p}_1$ projects out the factor $(\not{p}_1 - \not{l}_2)\not{p}_1 = -(l_2^- \gamma^+ + \not{l}_{2T})\not{p}_1$. Hence, the second line is infrared finite.

In the third line of (44) the x-derivative acts outside the l_2 integral, so l_1 can be off-shell. The Ward identity (A5) then leaves us with an additional piece

$$\left[\frac{l_1 \cdot S_T}{p_1 \cdot (p_2 - p_q)} + \frac{l_2 \cdot S_T}{p_1 \cdot (p_2 - l_2)}\right] \frac{N_c(N_c^2 - 1)}{4} \frac{l_1^2}{(l_1 - l_2)^2} \mathrm{Tr}\left[\gamma_5 \not{p}_1 A^{\alpha\mu} (\not{p}_1 - \not{l}_1)\gamma_\alpha (\not{p}_2 - \not{l}_2)\gamma^\nu \frac{\not{p}_1 - \not{l}_2}{(p_1 - l_2)^2} \frac{\gamma^+}{l_2^+}\right], \tag{A10}$$

where the $l_2 \cdot S_T$ term, being at least $O(l_{2T})$, is finite, while the $l_1 \cdot S_T$ term looks divergent. Applying $x\partial/\partial x$, we have the divergent remainder from the third line

$$\frac{N_c(N_c^2 - 1)}{2} \frac{l_1 \cdot S_T}{(l_1 - l_2)^2} \mathrm{Tr}\left[\gamma_5 \not{p}_1 A^{\alpha\mu} (\not{p}_2 - \not{l}_1)\gamma_\alpha (\not{p}_2 - \not{l}_2)\gamma^\nu \frac{\not{p}_1 - \not{l}_2}{(p_1 - l_2)^2} \frac{\gamma^+}{l_2^+}\right]. \tag{A11}$$

The fourth line can be divided into two parts. The first part, coming from the derivative $x\partial/\partial x$ hit on the $\not{p}_1 \bar{M}^\mu_\beta$ structure, contains a prefactor $l_2 \cdot S_T$ according to (A6) and is finite. The second part from the $x\partial/\partial x = p_1^\alpha \partial/\partial p_1^\alpha$ hit on the $p_1 - l_2$ propagator is given by

$$-p_1^\alpha \frac{\partial}{\partial p_1^\alpha} \frac{\not{p}_1 - \not{l}_2}{(p_1 - l_2)^2} = \frac{\not{p}_1 - \not{l}_2}{(p_1 - l_2)^2} \not{p}_1 \frac{\not{p}_1 - \not{l}_2}{(p_1 - l_2)^2}, \tag{A12}$$

with the $O(l_{2T}^4)$ denominator. The numerator $(\not{p}_1 - \not{l}_2)\not{p}_1(\not{p}_1 - \not{l}_2) = 2(p_1 \cdot l_2)\not{l}_2 = 2p_1^+ l_2^- \not{l}_2 \sim O(l_{2T}^2)$, together with the prefactor $l_2 \cdot S_T$, provides sufficient suppression at $l_{2T} \to 0$, so the fourth line is finite.

We can also split the fifth line into two parts, the extra piece from implementing the Ward identity (A7) and the remainder. The divergence in the piece proportional to $l_1 \cdot S_T$,

$$-\frac{N_c(N_c^2 - 1)}{4} \frac{2l_1 \cdot S_T}{(p_2 - p_q - l_2)^2} \mathrm{Tr}\left[\gamma_5 \not{p}_1 A^{\alpha\mu} \not{p}_q \gamma_\alpha (\not{p}_2 - \not{l}_2)\gamma^\nu \frac{\not{p}_1 - \not{l}_2}{(p_1 - l_2)^2} \frac{\gamma^+}{l_2^+}\right], \tag{A13}$$

is of the same form, but with an opposite sign to that of (A11). The remaining divergences are collected, after the cancellation between the third and fifth lines, by

$$
\begin{aligned}
&-\mathrm{Tr}\left[\gamma_5 \not{S}_T \bar{M}^{\mu}_{\beta}\gamma^{\nu}\frac{\not{p}_1-\not{l}_2}{(p_1-l_2)^2}\gamma^{\beta}\right]+\mathrm{Tr}\left[\gamma_5\not{p}_1\bar{M}^{\mu}_{\beta}\gamma^{\nu}\frac{\not{p}_1-\not{l}_2}{(p_1-l_2)^2}\not{S}_T\frac{\not{p}_1-\not{l}_2}{(p_1-l_2)^2}\gamma^{\beta}\right]\\
&=-\mathrm{Tr}\left[\gamma_5\not{S}_T\bar{M}^{\mu}_{i}\gamma^{\nu}\frac{(p_1^+-l_2^+)\gamma^-}{(p_1-l_2)^2}\gamma^i\right]+\mathrm{Tr}\left[\gamma_5\not{p}_1\bar{M}^{\mu}_{-}\gamma^{\nu}\frac{\not{p}_1-\not{l}_2}{(p_1-l_2)^2}\not{S}_T\frac{\not{p}_1-\not{l}_2}{(p_1-l_2)^2}\left(\gamma^- -\frac{l_2^-}{l_2^+}\gamma^+\right)\right]\\
&\quad+\mathrm{Tr}\left[\gamma_5\not{p}_1\bar{M}^{\mu}_{i}\gamma^{\nu}\frac{\not{p}_1-\not{l}_2}{(p_1-l_2)^2}\not{S}_T\frac{\not{p}_1-\not{l}_2}{(p_1-l_2)^2}\left(\gamma^i-\frac{l_2^i}{l_2^+}\gamma^+\right)\right],
\end{aligned}
\tag{A14}
$$

with the Ward identity (A8), where the first term in the second line and the third line involve the divergences.

The relation

$$
\frac{\not{p}_1-\not{l}_2}{(p_1-l_2)^2}\not{S}_T\frac{\not{p}_1-\not{l}_2}{(p_1-l_2)^2}=-2(l_2\cdot S_T)\frac{\not{p}_1-\not{l}_2}{(p_1-l_2)^4}-\frac{\not{S}_T}{(p_1-l_2)^2},
\tag{A15}
$$

and the multiplication by $\not{p}_1$ on the left lead the third line of (A14) to

$$
\begin{aligned}
\left[-2(l_2\cdot S_T)\frac{\not{p}_1-\not{l}_2}{(p_1-l_2)^4}-\frac{\not{S}_T}{(p_1-l_2)^2}\right]\left(\gamma^i-\frac{l_2^i}{l_2^+}\gamma^+\right)&=2(l_2\cdot S_T)\frac{\not{l}_{2T}}{(p_1-l_2)^4}\gamma^i+2(l_2\cdot S_T)\frac{l_2^i}{l_2^+}\frac{p_1^+-l_2^+}{(p_1-l_2)^4}\gamma^-\gamma^+-\frac{1}{(p_1-l_2)^2}\not{S}_T\gamma^i\\
&=-l_{2T}^2\frac{\not{S}_T}{(p_1-l_2)^4}\gamma^i-\mathbf{l}_{2T}^2\frac{S_T^i}{l_2^+}\frac{p_1^+-l_2^+}{(p_1-l_2)^4}\gamma^-\gamma^+-\frac{1}{(p_1-l_2)^2}\not{S}_T\gamma^i\\
&=-\frac{p_1^+-l_2^+}{p_1^+}\frac{1}{(p_1-l_2)^2}(\not{S}_T\gamma^i+S_T^i\gamma^-\gamma^+).
\end{aligned}
\tag{A16}
$$

where the angular average has been performed for the second expression, and $l_{2T}^2=2l_2^+l_2^-$ has been inserted into the third expression. Multiplying the last expression by $\not{p}_1$ in the trace on the right and using $\not{S}_T\gamma^i\gamma^- - S_T^i\gamma^-\gamma^+\gamma^- = -\gamma^-\gamma^i\not{S}_T$, we arrive at

$$
-\left[2(l_2\cdot S_T)\frac{\not{p}_1-\not{l}_2}{(p_1-l_2)^4}+\frac{\not{S}_T}{(p_1-l_2)^2}\right]\left(\gamma^i-\frac{l_2^i}{l_2^+}\gamma^+\right)\not{p}_1=\frac{(p_1^+-l_2^+)\gamma^-}{(p_1-l_2)^2}\gamma^i\not{S}_T.
\tag{A17}
$$

The divergent piece in third line of (A14) is thus reduced to the same form as the first term in the second line of (A14), but has an opposite sign. That is, the divergences in (A14) cancel each other. In conclusion, the l_2 integral in (44) is infrared finite, and we can safely proceed to its numerical evaluation.

APPENDIX B: ANALYSIS OF INFRARED DIVERGENCES: GLUON-INITIATED CHANNEL

The gluon-initiated differential cross section (63) has two potential sources of infrared divergences from the p_1-l_2 and $q-l_2$ quark propagators in (61). The p_1-l_2 propagator in $A_{\nu\beta}$ causes a divergence as $(p_1-l_2)^2=-2p_1^+l_2^-\propto l_{2T}^2\to 0$ [corresponding to $a_2=+1$ in (48)]. With the multiplication of $\not{l}_2$ on the right, as indicated by the γ-matrix indices in (59), the divergent piece in the second line of (63) is proportional to

$$
A_{\nu\beta}\not{l}_2\to\gamma_\nu\frac{\not{p}_1-\not{l}_2}{(p_1-l_2)^2}\gamma_\beta\not{l}_2\to 2l_2^+\delta_{\beta-}\gamma_\nu\frac{(p_1^+-l_2^+)\gamma^-}{(p_1-l_2)^2},
\tag{B1}
$$

where $\beta=-$ has been singled out. One can easily check that a divergence is not produced due to $l_2^-\propto l_{2T}^2$ in the numerator when β is transverse. In the third line, β is transverse and there is no divergence for the same reason. The derivative $x\partial/\partial x$ acts outside of the l_{2T} integral in the fourth line, so we evaluate the integral and take the derivative afterwards. It is then seen that there is no divergence, for β is also transverse. In the fifth line we take the derivative first, which, as hitting $A_{\alpha\mu}\bar{M}$, does not induce a divergence since β is transverse. When it hits $A_{\nu\beta}$, we have

$$
x\frac{\partial}{\partial x}A_{\nu\beta}\to-\gamma_\nu\frac{\not{p}_1-\not{l}_2}{(p_1-l_2)^2}\not{p}_1\frac{\not{p}_1-\not{l}_2}{(p_1-l_2)^2}\gamma_\beta.
\tag{B2}
$$

With $(\not{p}_1 - \not{l}_2)\not{p}_1(\not{p}_1 - \not{l}_2) \sim O(l_{2T}^2)$ and the prefactor going as $O(l_{2T})$, the numerator in total behaves like $O(l_{2T}^3)$, such that the l_{2T} integral is finite.

In the sixth line, when $\partial/\partial k^\lambda$ hits $A_{\alpha\mu}\bar{M}$, the result is finite because β is transverse. When it hits $A_{\nu\beta}$, we get

$$\frac{\partial}{\partial k^\lambda} A_{\nu\beta} \to -\gamma_\nu \frac{\not{p}_1 - \not{l}_2}{(p_1 - l_2)^2}\gamma_\lambda \frac{\not{p}_1 - \not{l}_2}{(p_1 - l_2)^2}\gamma_\beta = 2l_{2\lambda}\gamma_\nu \frac{\not{p}_1 - \not{l}_2}{(p_1 - l_2)^4}\gamma_\beta + \gamma_\nu\gamma_\lambda\gamma_\beta \frac{1}{(p_1 - l_2)^2}. \tag{B3}$$

The multiplication by $\not{l}_2$ on the right yields

$$\frac{\partial}{\partial k^\lambda} A_{\nu\beta}\not{l}_2 \to -2l_2^+ \delta_{\lambda\beta} \frac{1}{p_1^+}\gamma_\nu \frac{(p_1^+ - l_2^+)\gamma^-}{(p_2 - l_1)^2}, \tag{B4}$$

where we have performed the angular average and inserted $l_{2T}^2 = 2l_2^+ l_2^-$. The total contribution then goes as

$$\begin{aligned} &-\frac{1}{x}\epsilon^{nP\alpha S_T}\hat{S}^{(0)}_{\mu\nu\alpha-}\frac{1}{P^+} - (g_T^{\beta\lambda}\epsilon^{\alpha PnS_T} - g_T^{\alpha\lambda}\epsilon^{\beta PnS_T})\left[\frac{\partial}{\partial k^\lambda}\hat{S}^{(0)}_{\mu\nu\alpha\beta}(k)\right]_{k=p_1} \\ &\quad\to -\epsilon^{nP\alpha S_T} 2l_2^+ \frac{1}{p_1^+}\gamma_\nu \frac{(p_1^+ - l_2^+)\gamma^-}{(p_1 - l_2)^2} + (g_T^{\beta\lambda}\epsilon^{\alpha PnS_T} - g_T^{\alpha\lambda}\epsilon^{\beta PnS_T})2l_2^+\delta_{\lambda\beta}\frac{1}{p_1^+}\gamma_\nu \frac{(p_1^+ - l_2^+)\gamma^-}{(p_1 - l_2)^2} = 0. \end{aligned} \tag{B5}$$

That is, even though the second and sixth lines are separately divergent when $l_2^+ \to p_2^+$ and $l_2^-, l_{2T} \to 0$, there is no infrared divergence in their sum.

Next we come to the potential divergence in the $q - l_2$ quark propagator [corresponding to $a_2 = -1$ in (48)], whose denominator $(q - l_2)^2 = -2p_1 \cdot (p_2 - l_2) = -2p_1^+(p_2^- - l_2^-)$ with $(p_2 - l_2)^2 = 0$ diminishes when $l_2^- \to p_2^-$ and $l_2^+, l_{2T} \to 0$. The divergent piece in the second line of (63) is identified as

$$(\not{p}_2 - \not{l}_2)A_{\nu\beta} \to 2p_2^+\delta_{\beta-}\frac{q^+\gamma^-}{(q - l_2)^2}\gamma_\nu, \tag{B6}$$

which, together with the overall prefactors, gives

$$-\epsilon^{nP\alpha S_T}\frac{1}{x}\hat{S}^{(0)}_{\mu\nu\alpha-} \to \frac{2p_2^+}{p_1^+}\epsilon^{\alpha PnS_T}\frac{q^+\gamma^-}{(q - l_2)^2}\gamma_\nu. \tag{B7}$$

The third line is finite as before. In the fourth line, β is transverse in $\hat{S}^{(0)}$, but the prefactor now goes as $O(1/l_{2T})$. Since the derivative $x\partial/\partial x$ acts outside the l_{2T} integral, we first evaluate the δ-function, obtaining the relevant piece

$$\frac{\partial}{\partial x}\left[x\frac{l_{2T}^\beta\epsilon^{\alpha PnS_T} - l_{2T}^\alpha\epsilon^{\beta PnS_T}}{p_1 \cdot (p_2 - l_2)}(\not{p}_2 - \not{l}_2)A_{\nu\beta}\right]. \tag{B8}$$

Due to the condition $(p_2 - l_2)^2 = 0$, l_2 also depends on x, in addition to p_1. The relation

$$x\frac{\partial l_2^\mu}{\partial x} = \frac{1}{2}\frac{p_1^+}{p_2^+}\tilde{l}_2^\mu, \qquad \tilde{l}_2^\mu = (2l_2^+, 0, \vec{l}_{2T}), \tag{B9}$$

then leads (B8) to

$$\begin{aligned} &x\frac{\partial}{\partial x}[(l_{2T}^\beta\epsilon^{\alpha PnS_T} - l_{2T}^\alpha\epsilon^{\beta PnS_T})(\not{p}_2 - \not{l}_2)A_{\nu\beta}] \\ &\quad = (l_{2T}^\beta\epsilon^{\alpha PnS_T} - l_{2T}^\alpha\epsilon^{\beta PnS_T})\left[\not{p}_1 A_{\nu\beta} + \left(-1 + \frac{1}{2}\frac{p_1^+}{p_2^+}\right)(\not{p}_2 - \not{l}_2)A_{\nu\beta} - \frac{1}{2}\frac{p_1^+}{p_2^+}\tilde{\not{l}}_2 A_{\nu\beta} - \frac{1}{2}\frac{p_1^+}{p_2^+}\gamma_\beta\frac{\tilde{\not{l}}_2}{(q - l_2)^2}\gamma_\nu\right], \end{aligned} \tag{B10}$$

viewing that the factor $x/p_1 \cdot (p_2 - l_2)$ is independent of x. In the fifth line, the x-derivative acts inside the l_2 integral, so the only effect is

$$x\frac{\partial}{\partial x}(\not{p}_2 - \not{l}_2)A^{\nu}{}_{\beta} = \not{p}_1 A^{\nu}{}_{\beta}, \tag{B11}$$

which cancels the first term in the square brackets on the right-hand side of (B10). Therefore, we focus on the remaining terms in the fourth line,

$$\begin{aligned}&\frac{l_{2T}^{\beta}\epsilon^{\alpha PnS_T} - l_{2T}^{\alpha}\epsilon^{\beta PnS_T}}{p_1\cdot(p_2-l_2)}\left[\left(-1+\frac{1}{2}\frac{p_1^+}{p_2^+}\right)(\not{p}_2-\not{l}_2)A_{\nu\beta} - \frac{1}{2}\frac{p_1^+}{p_2^+}\tilde{\not{l}}_2 A_{\nu\beta} - \frac{1}{2}\frac{p_1^+}{p_2^+}\gamma_\beta\frac{\tilde{\not{l}}_2}{(q-l_2)^2}\gamma_\nu\right]\\ &\quad\to\left[2\left(1-\frac{p_2^+}{p_1^+}\right)\epsilon^{\alpha PnS_T} - \epsilon^{\beta PnS_T}\gamma^\alpha\gamma_\beta\right]\frac{q^+\gamma^-}{(q-l_2)^2}\gamma_\nu.\end{aligned} \tag{B12}$$

The sixth line contributes

$$(g_T^{\beta\lambda}\epsilon^{\alpha PnS_T} - g_T^{\alpha\lambda}\epsilon^{\beta PnS_T})\left\{\frac{\partial}{\partial k^\lambda}[(\not{k}+\not{q}-\not{l}_2)A_{\nu\beta}]\right\}_{k=p_1} \to (2\epsilon^{\alpha PnS_T} - \epsilon^{\beta PnS_T}\gamma^\alpha\gamma_\beta)\frac{q^+\gamma^-}{(q-l_2)^2}\gamma_\nu. \tag{B13}$$

It is clear that the divergences in the fourth and sixth lines cancel up to a piece

$$-\frac{2p_2^+}{p_1^+}\epsilon^{\alpha PnS_T}\frac{q^+\gamma^-}{(q-l_2)^2}\gamma_\nu, \tag{B14}$$

which is exactly what we need to cancel the divergence in the second line in (B7). In conclusion, the l_2 integral in (63) is infrared finite, and we can safely proceed to its numerical evaluation.

APPENDIX C: USEFUL INTEGRALS

In this Appendix we list the integrals over ϕ_2 (azimuthal angle of the parton with momentum l_2) that we have employed in the calculation of the hard coefficients:

$$\begin{aligned}\int_0^{2\pi} d\phi_2 \frac{1}{a+b\cos(\phi_1-\phi_2)} &= \frac{2\pi\,\mathrm{sgn}(a)}{\sqrt{a^2-b^2}},\\ \int_0^{2\pi} d\phi_2 \frac{1}{(a+b\cos(\phi_1-\phi_2))^2} &= \frac{2\pi|a|}{(a^2-b^2)^{3/2}},\\ \int_0^{2\pi} d\phi_2 \frac{\sin(\phi_2-\Phi_S)}{a+b\cos(\phi_1-\phi_2)} &= \frac{2\pi}{b}\sin(\phi_1-\Phi_S)\left(1-\frac{|a|}{\sqrt{a^2-b^2}}\right),\\ \int_0^{2\pi} d\phi_2 \frac{\sin(\phi_2-\Phi_S)}{(a+b\cos(\phi_1-\phi_2))^2} &= -2\pi b\sin(\phi_1-\Phi_S)\frac{\mathrm{sgn}(a)}{(a^2-b^2)^{3/2}},\\ \int_0^{2\pi} d\phi_2 \frac{\cos(\phi_2-\Phi_S)}{a+b\cos(\phi_1-\phi_2)} &= \frac{2\pi}{b}\cos(\phi_1-\Phi_S)\left(1-\frac{|a|}{\sqrt{a^2-b^2}}\right),\\ \int_0^{2\pi} d\phi_2 \frac{\cos(\phi_2-\Phi_S)}{(a+b\cos(\phi_1-\phi_2))^2} &= -2\pi b\cos(\phi_1-\Phi_S)\frac{\mathrm{sgn}(a)}{(a^2-b^2)^{3/2}}.\end{aligned} \tag{C1}$$

[1] S. Benic, Y. Hatta, H.-N. Li, and D.-J. Yang, Phys. Rev. D **100**, 094027 (2019).
[2] P. G. Ratcliffe, Nucl. Phys. **B264**, 493 (1986).
[3] A. V. Efremov and O. V. Teryaev, Sov. J. Nucl. Phys. **36**, 140 (1982).
[4] J.-W. Qiu and G. F. Sterman, Phys. Rev. D **59**, 014004 (1998).
[5] S. Wandzura and F. Wilczek, Phys. Lett. **72B**, 195 (1977).
[6] D. Pitonyak, Int. J. Mod. Phys. A **31**, 1630049 (2016).

[7] J. Cammarota, L. Gamberg, Z.-B. Kang, J. A. Miller, D. Pitonyak, A. Prokudin, T. C. Rogers, and N. Sato (Jefferson Lab Angular Momentum Collaboration), Phys. Rev. D **102**, 054002 (2020).
[8] X.-D. Ji, Phys. Lett. B **289**, 137 (1992).
[9] Y. Hatta, K. Tanaka, and S. Yoshida, J. High Energy Phys. 02 (2013) 003.
[10] Z.-B. Kang and J.-W. Qiu, Phys. Rev. D **78**, 034005 (2008).
[11] H. Beppu, Y. Koike, K. Tanaka, and S. Yoshida, Phys. Rev. D **82**, 054005 (2010).
[12] Y. Koike, K. Tanaka, and S. Yoshida, Phys. Rev. D **83**, 114014 (2011).
[13] A. Prokudin, Y. Hatta, Y. Kovchegov and C. Marquet, *Proceedings, Probing Nucleons and Nuclei in High Energy Collisions: Dedicated to the Physics of the Electron Ion Collider: Seattle (WA), United States, October 1–November 16, 2018* (WSP, 2020), https://doi.org/10.1142/11684.
[14] R. A. Khalek *et al.*, arXiv:2103.05419.
[15] C. Adolph *et al.* (COMPASS Collaboration), Phys. Lett. B **744**, 250 (2015).
[16] A. Bacchetta, U. D'Alesio, M. Diehl, and C. A. Miller, Phys. Rev. D **70**, 117504 (2004).
[17] R.-B. Meng, F. I. Olness, and D. E. Soper, Nucl. Phys. **B371**, 79 (1992).
[18] K. Kanazawa and Y. Koike, Phys. Rev. D **88**, 074022 (2013).
[19] H. Eguchi, Y. Koike, and K. Tanaka, Nucl. Phys. **B763**, 198 (2007).
[20] H. Eguchi, Y. Koike, and K. Tanaka, Nucl. Phys. **B752**, 1 (2006).
[21] X. Ji, J.-W. Qiu, W. Vogelsang, and F. Yuan, Phys. Lett. B **638**, 178 (2006).
[22] Y. Koike, K. Yabe, and S. Yoshida, Phys. Rev. D **101**, 054017 (2020).
[23] Y. Hatta, K. Kanazawa, and S. Yoshida, Phys. Rev. D **88**, 014037 (2013).
[24] H. Xing and S. Yoshida, Phys. Rev. D **100**, 054024 (2019).
[25] V. Shtabovenko, R. Mertig, and F. Orellana, Comput. Phys. Commun. **256**, 107478 (2020).
[26] J. C. Collins, D. E. Soper, and G. F. Sterman, Nucl. Phys. **B250**, 199 (1985).
[27] E. R. Nocera, R. D. Ball, S. Forte, G. Ridolfi, and J. Rojo (NNPDF Collaboration), Nucl. Phys. **B887**, 276 (2014).
[28] R. A. Khalek, V. Bertone, and E. R. Nocera, Phys. Rev. D **104**, 034007 (2021).
[29] J. J. Ethier, N. Sato, and W. Melnitchouk, Phys. Rev. Lett. **119**, 132001 (2017).
[30] H. H. Matevosyan, A. Kotzinian, E.-C. Aschenauer, H. Avakian, and A. W. Thomas, Phys. Rev. D **92**, 054028 (2015).
[31] M. G. Echevarria, Z.-B. Kang, and J. Terry, J. High Energy Phys. 01 (2021) 126.
[32] A. Bacchetta, M. Diehl, K. Goeke, A. Metz, P. J. Mulders, and M. Schlegel, J. High Energy Phys. 02 (2007) 093.
[33] W. Mao, Z. Lu, and B.-Q. Ma, Phys. Rev. D **90**, 014048 (2014).
[34] X. Wang and Z. Lu, Phys. Rev. D **93**, 074009 (2016).
[35] H. Beppu, K. Kanazawa, Y. Koike, and S. Yoshida, Phys. Rev. D **89**, 034029 (2014).
[36] G. L. Kane, J. Pumplin, and W. Repko, Phys. Rev. Lett. **41**, 1689 (1978).
[37] Y. V. Kovchegov and M. D. Sievert, Phys. Rev. D **86**, 034028 (2012); **86**, 079906(E) (2012).